VTRC
Virginia Transportation Research Council

We Bring Innovation to Transportation

Durability and Inspection of Hybrid Composite Beams

http://www.virginiadot.org/vtrc/main/online_reports/pdf/20-r7.pdf

SOUNDAR S.G. BALAKUMARAN, Ph.D., P.E.
Associate Director

STEPHEN R. SHARP, Ph.D., P.E.
Senior Research Scientist

Final Report VTRC 20-R7

VIRGINIA TRANSPORTATION RESEARCH COUNCIL
530 Edgemont Road, Charlottesville, VA 22903-2454
vtrc.virginiadot.org

Standard Title Page - Report on Federally Funded Project

1. Report No.: FHWA/VTRC 20-R7	2. Government Accession No.:	3. Recipient's Catalog No.:
4. Title and Subtitle: Durability and Inspection of Hybrid Composite Beams		5. Report Date: September 2019
		6. Performing Organization Code:
7. Author(s): Soundar S.G. Balakumaran, Ph.D., P.E., and Steven R. Sharp, Ph.D., P.E.		8. Performing Organization Report No.: VTRC 20-R7
9. Performing Organization and Address: Virginia Transportation Research Council 530 Edgemont Road Charlottesville, VA 22903		10. Work Unit No. (TRAIS):
		11. Contract or Grant No.: 106882
12. Sponsoring Agencies' Name and Address: Virginia Department of Transportation 1401 E. Broad Street Richmond, VA 23219 Federal Highway Administration 400 North 8th Street, Room 750 Richmond, VA 23219-4825		13. Type of Report and Period Covered: Final
		14. Sponsoring Agency Code:
15. Supplementary Notes:		

16. Abstract:

The ability to inspect reasonably and ensure the durability of hybrid composite beams (HCBs) is of concern to transportation agencies. In case of infiltration of chloride-laden water through the fiber-reinforced polymer (FRP) shell of an HCB, tension reinforcement strands in the bottom flange will be subject to corrosion, thus severely affecting the service life of the beams. Test specimens from HCBs, which were load tested to failure at Virginia Tech for a 2012 study, and specimens manufactured for testing by HCB, Inc., were used in this study. A selected number of specimens were subjected to accelerated exposure in the laboratory by exposure to ultraviolet radiation and condensation cycles. In addition, to compare the influence of actual field exposure, specimens were placed in two selected field locations with different exposure conditions. All specimens were characterized before and, periodically, during the exposure using nondestructive and destructive methods to understand the change over time. The specimens were photographed periodically during the study to identify any progress of deterioration.

Ground penetrating radar was found to be reliable in detecting moisture in the interior of HCBs. Fourier transform infrared spectroscopy was used to understand the changes in the chemical structure of the exposed specimens. Spectrocolorimetry was used to understand the natural changes in the surface conditions of the FRP shell as the exposure duration progressed. The literature review provided extensive information on the aging behavior of the FRP shell specimens.

The greatest degree of damage was found at the field exposure site with the highest recorded UV index values. Based on the preliminary results, HCB specimens with no preexisting blemishes have exhibited only minor degradation in the course of laboratory and field exposures. The specimens with preexisting damages such as delaminations, scratches, and other blemishes have degraded more rapidly than have the sound specimens. None of the beam components exhibited complete failure after 1 year and 8 months of outdoor atmospheric exposure.

Scanning electron microscopy and X-ray computed tomography provided excellent visualization of the surface and the volume, respectively, of the FRP material to demonstrate the fiber layout. Tensile testing of the FRP specimens indicated the importance of the fiber content in the FRP specimens. Resin degradation because of natural ultraviolet and freeze-thaw degradation and accidental damages because of flooding events should be repaired to protect the load-carrying fiber content. At this stage, regarding findings related to durability, the Virginia Department of Transportation should pause further use of HCBs, since there are still many unknowns about the late-stage deterioration mechanism of FRP, and also because neither visual nor nondestructive methods can fully assess the condition of the beams at this time. Further environmental exposure is recommended for a reliable sense of HCB durability.

17 Key Words: Hybrid-composite beam, Hillman beam, FRP, vinyl ester, glass fiber, FTIR, XCT, SEM, accelerated aging, spectrocolorimetry	18. Distribution Statement: No restrictions. This document is available to the public through NTIS, Springfield, VA 22161.

19. Security Classif. (of this report): Unclassified	20. Security Classif. (of this page): Unclassified	21. No. of Pages: 47	22. Price:

FINAL REPORT

DURABILITY AND INSPECTION OF HYBRID COMPOSITE BEAMS

Soundar S.G. Balakumaran, Ph.D., P.E.
Associate Director

Stephen R. Sharp, Ph.D., P.E.
Senior Research Scientist

In Cooperation with the U.S. Department of Transportation
Federal Highway Administration

Virginia Transportation Research Council
(A partnership of the Virginia Department of Transportation
and the University of Virginia since 1948)

Charlottesville, Virginia

September 2019
VTRC 20-R7

DISCLAIMER

The contents of this report reflect the views of the authors, who are responsible for the facts and the accuracy of the data presented herein. The contents do not necessarily reflect the official views or policies of the Virginia Department of Transportation, the Commonwealth Transportation Board, or the Federal Highway Administration. This report does not constitute a standard, specification, or regulation. Any inclusion of manufacturer names, trade names, or trademarks is for identification purposes only and is not to be considered an endorsement.

ABSTRACT

The ability to inspect reasonably and ensure the durability of hybrid composite beams (HCBs) is of concern to transportation agencies. In case of infiltration of chloride-laden water through the fiber-reinforced polymer (FRP) shell of an HCB, tension reinforcement strands in the bottom flange will be subject to corrosion, thus severely affecting the service life of the beams. Test specimens from HCBs, which were load tested to failure at Virginia Tech for a 2012 study, and specimens manufactured for testing by HCB, Inc., were used in this study. A selected number of specimens were subjected to accelerated exposure in the laboratory by exposure to ultraviolet radiation and condensation cycles. In addition, to compare the influence of actual field exposure, specimens were placed in two selected field locations with different exposure conditions. All specimens were characterized before and, periodically, during the exposure using nondestructive and destructive methods to understand the change over time. The specimens were photographed periodically during the study to identify any progress of deterioration.

Ground penetrating radar was found to be reliable in detecting moisture in the interior of HCBs. Fourier transform infrared spectroscopy was used to understand the changes in the chemical structure of the exposed specimens. Spectrocolorimetry was used to understand the natural changes in the surface conditions of the FRP shell as the exposure duration progressed. The literature review provided extensive information on the aging behavior of the FRP shell specimens.

The greatest degree of damage was found at the field exposure site with the highest recorded UV index values. Based on the preliminary results, HCB specimens with no preexisting blemishes have exhibited only minor degradation in the course of laboratory and field exposures. The specimens with preexisting damages such as delaminations, scratches, and other blemishes have degraded more rapidly than have the sound specimens. None of the beam components exhibited complete failure after 1 year and 8 months of outdoor atmospheric exposure.

Scanning electron microscopy and X-ray computed tomography provided excellent visualization of the surface and the volume, respectively, of the FRP material to demonstrate the fiber layout. Tensile testing of the FRP specimens indicated the importance of the fiber content in the FRP specimens. Resin degradation because of natural ultraviolet and freeze-thaw degradation and accidental damages because of flooding events should be repaired to protect the load-carrying fiber content. At this stage, regarding findings related to durability, the Virginia Department of Transportation should pause further use of HCBs, since there are still many unknowns about the late-stage deterioration mechanism of FRP, and also because neither visual nor nondestructive methods can fully assess the condition of the beams at this time. Further environmental exposure is recommended for a reliable sense of HCB durability.

FINAL REPORT

DURABILITY AND INSPECTION OF HYBRID COMPOSITE BEAMS

Soundar S.G. Balakumaran, Ph.D., P.E.
Associate Director

Stephen R. Sharp, Ph.D., P.E.
Senior Research Scientist

INTRODUCTION

In 2015, the U.S. Department of Transportation (2015) reported that an estimated annual average funding of $89.9 billion was needed to maintain the conditions and performance of the nationwide transportation infrastructure. The funding needed to improve conditions and performance was estimated at $142.5 billion annually. In Virginia, according to the Virginia Department of Transportation (VDOT) Dashboard in 2009, 7% of bridges and culverts were structurally deficient (VDOT, 2009). With the number of structures needing major rehabilitation and replacement increasing along with the associated costs, it makes sense to think in terms of the overall life cycle of structures rather than the initial investment alone. Cheaper construction materials that are vulnerable to corrosion and other forms of deterioration will require significant funds for maintenance in the long term. In addition, construction materials and systems that are conducive to faster construction can reduce the user costs involved in traffic control during construction and maintenance activities.

Hybrid composite beams (HCBs) may be a viable alternative to some currently used precast bridge superstructures. The HCB, originally designed by Hillman, is an innovative design consisting of three components (Hillman, 2003; Hillman, 2008). The compression stress-bearing component is the internal concrete arch, which runs from end to end on the beam. The tension-reinforcing component consists of metallic or nonmetallic ropes that tie the legs of the concrete arch. The outermost component is a fiber-reinforced polymer (FRP) shell, which encapsulates the innards and prevents moisture and salt from infiltrating. The shell is made up of vinyl ester resin reinforced by glass fibers oriented to resist appropriate forces (Hillman, 2003). This resin matrix was selected mainly based on the selection of glass fibers and the intended fabrication process. The spaces inside the FRP shell outside the arch are filled with a rigid foam material.

The main advantage of an HCB is the FRP outer shell, which protects the concrete and reinforcement from exposure to harmful chemicals. Placement of concrete into the arch can be performed either in the casting yard before transportation or after installation at the site of the bridge. In the latter case, the lightness of the unfilled shell may be an added advantage for transport and erection. Even after the arch is filled with concrete, the weight of an HCB is one-fifth that of a steel beam and one-tenth that of a precast prestressed concrete beam designed for the same span length (Hillman, 2003).

PURPOSE AND SCOPE

The purpose of this study was to determine the general durability of HCBs and the factors affecting them using advanced material evaluation techniques such as Fourier transform infrared spectroscopy (FTIR), scanning electron microscopy (SEM), and X-ray computed tomography (XCT). The study plan was to document the incidence of deterioration of the fiberglass shell and the effects on the durability of strands. In addition, since HCBs are more difficult to inspect, appropriate nondestructive techniques were evaluated for effectiveness.

The scope of the study was accelerated laboratory exposure and field exposure of the FRP shell material and evaluation of the factors affecting its durability. All specimens were to be characterized before exposure and, periodically, during the exposure using nondestructive and destructive methods to quantify the damage over time.

METHODS

The study included the following tasks:

1. Compile information from the literature regarding the performance of the materials used in the manufacture of HCBs.

2. Conduct accelerated exposure using ultraviolet (UV) exposure in the laboratory and monitor the condition of the FRP specimens periodically.

3. Conduct field exposure of the FRP specimens in different environments and monitor the condition of the specimens periodically.

4. Evaluate the specimens at the end of the laboratory and field exposures using destructive tensile strength testing and nondestructive techniques to understand the level of deterioration.

Task 1: Literature Review

A literature review was conducted using library resources and Google Scholar searches. The keywords used for the searches were vinyl eater resin, glass fibers, UV degradation, durability of vinyl ester, weathering, accelerated aging, and scanning electron microscope.

Task 2: Laboratory Accelerated Exposure

Both laboratory and field exposures of HCB specimens were conducted, since the correlation between the results of laboratory accelerated aging and the actual field performance of composites remains debatable.

Specimens for exposure testing were fashioned from the bottom flange of HCBs after the beams were load tested to failure at Virginia Tech as a part of a study by Ahsan (2012). One of the bottom flanges used in the study is shown in Figure 1.

Four types of specimens were prepared for various testing necessities, as described in Table 1. FRP, FRP with exposed steel strands, and foam were shaped from an HCB.

The FRP specimens were aged in the laboratory with UV radiation and condensation. Accelerated UV exposure was conducted using a QUV accelerated weathering tester (Figure 2) in accordance with ASTM D4587 (ASTM International [ASTM], 2011). Cycle 4, as prescribed in the standard, was used. Cycle 4 consists of a 0.89 W/m^2.nm UV radiation intensity at a 340 nm wavelength for 8 hr at 60 °C followed by 4 hr of condensation at 50 °C.

The space within the QUV accelerated weathering machine allowed 28 FRP specimens and 4 thin foam specimens with dimensions of 5 x 4 in. The laboratory UV exposure was interrupted at 920 hr and 2000 hr for colorimetry, FTIR, and digital imaging.

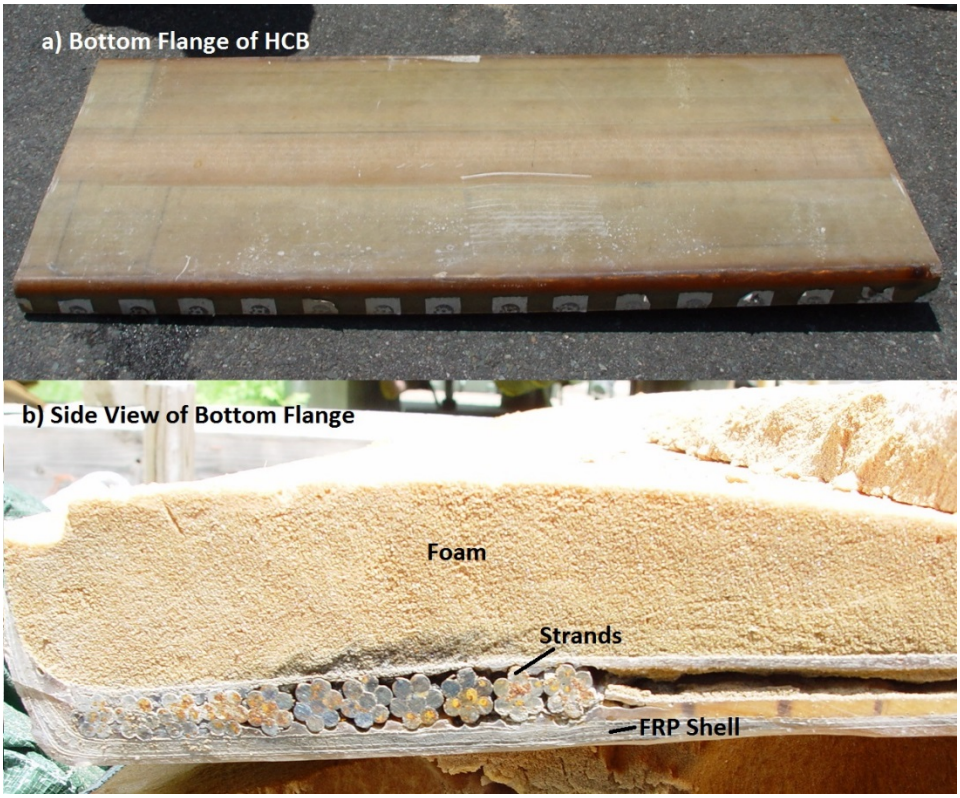

Figure 1. Hybrid Composite Beam: (a) bottom flange; b) side view of bottom flange. HCB = hybrid composite beam; FRP = fiber-reinforced polymer.

Figure 2. Accelerated Weathering Machine

FTIR

FTIR is a near-surface evaluation technique that shines waves with a wide range of frequencies in the infrared spectrum on the target material and measures the reflected or emitted frequencies. The information is converted into a spectrum using the Fourier transform. Advantages of this system include a broad scan of a wide spectrum and near-instant measurements. However, the presence of impurities can easily add noise to the readings.

This method involves simple data collection followed by an advanced data analysis and then an even more advanced data interpretation. This method will not work as a routine inspection technique, considering the expense of the equipment and expertise needed in addition to the aforementioned reasons. This method was used as a research tool only for an in-depth understanding of the change in the material property when exposed to different weathering factors. A handheld Agilent 4100 ExoScan Series FTIR was used in this study, as shown in Figure 3.

Figure 3. Fourier Transform Infrared Spectroscopy Equipment

Colorimetry

One of the objectives of this study was to find a simpler but reliable way to inspect the condition of the FRP material. Thus, considering the nature of the degradation of the FRP composite materials that involves chemical changes, which changes the color of the material over time, a careful visual inspection could work. In order to quantify the color change without the subjectivity of human factors, several methods were considered. Finally, colorimetry was selected based on the simplicity of the data collection and interpretation and the cost of the equipment.

Colorimetry is the quantification of human color perception. The spectrum is thus limited to the visual electromagnetic wavelength range of 400 to 700 nm. The color system used was the International Commission on Illumination's (or Commission Internationale de l'Eclairage) CIE L*a*b* and CIE L*C*h° color spaces.

CIE L*a*b* uses Cartesian or rectangular coordinates (Schwiegerling, 2004):

- L* is the vertical axis, and a* and b* are in the perpendicular plane, perpendicular to each other. L* stands for lightness, which runs from 0 to 100, where 0 represents the darkest black and 100 represents the brightest white.

- a* stands for the color between green and red, where green is represented by negative numbers and red is represented by positive numbers.

- b* stands for the color between blue and yellow, where blue is represented by negative numbers and yellow is represented by positive numbers. True neutral gray values are represented by a* = b* = 0.

CIE L*C*h° uses cylindrical coordinates:

- L* is the vertical axis, the same as in the L*a*b* color space.

- C* stands for Chroma or saturation, which is the distance from the L* axis in the perpendicular plane. Chroma is a positive number that starts with 0, where 0 stands for neutral or unsaturated gray and 100 stands for high saturation or color purity.

- h° stands for hue, which represents the circumference of the cylinder with fully saturated colors at the edge of the circle; hue angle is 0° at red, 90° at yellow, 180° at green, and 270° at blue.

For consistency, the measurements were made at D65 illumination, which is an international lighting standard. D65 represents a standard daylight condition at 6504 K color temperature. In addition, the field of vision was taken to be 10°, which represents the standard human field of view. An X-Rite RM200QC Imaging Spectrocolorimeter was used in this study. Figure 4 shows the spectrocolorimeter.

Figure 4. Spectrocolorimeter

Task 3: Field Exposure

Two field exposure sites were selected in Virginia to understand the natural weathering process of this material. The sites were in Hampton Roads and Harrisonburg, shown in Figure 5, where Hampton Roads represents severe coastal conditions, and Harrisonburg represents a mild exposure rural environment.

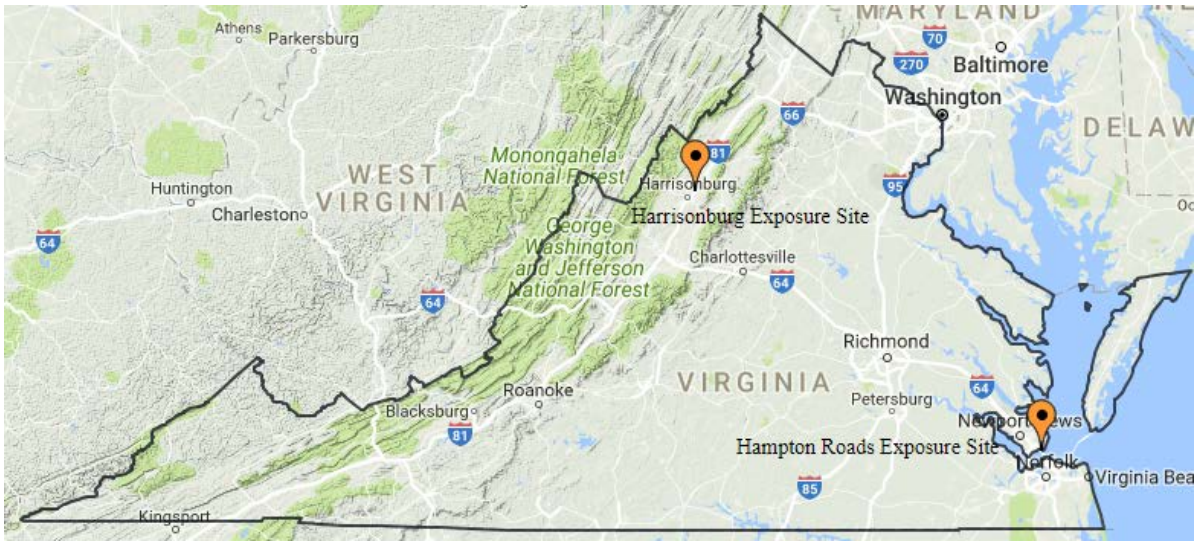

Figure 5. Field Exposure Sites

FRP with protected steel specimens was manufactured by HCB, Inc., for this study. Table 1 shows the number of specimens that were placed at the two exposure sites, and the mid-preparation of the specimens is shown in Figure 6.

Table 1. Test Materials Evaluated During This Study

Material	Description	No. of Specimens Placed at Hampton Roads Exposure Site	No. of Specimens Placed at Harrisonburg Exposure Site
FRP	FRP without strand or foam	12	12
FRP with exposed steel	FRP with strand end exposed	4	4
FRP with protected steel	FRP with strand fully encapsulated	5	5
Foam	Foam directly exposed	3	3

FRP = fiber-reinforced polymer.

Figure 6. Hybrid Composite Beam Specimens Under Preparation

The Harrisonburg and Hampton Roads exposure panels are shown in Figures 7 and 8, respectively.

Figure 7. Harrisonburg Exposure Site

Figure 8. Hampton Roads Exposure Site

Weather stations were placed at the Harrisonburg and Hampton Roads sites to gather weather data. These stations were placed near the specimens to collect temperature, humidity, precipitation, solar radiation, and UV index data. A wind vane was mounted at 7 ft and a rain cone was mounted at 5 ft above the ground. The resolution and accuracy of each sensor are provided in Table 2.

Table 2. Sensor Resolution and Accuracy

Weather Data Element	Data Resolution	Accuracy of Measurement
Temperature	0.1 °F	1 °F
Humidity	1%	3% relative humidity, 4% above 90%
Precipitation	0.01 in	Greater than 4%
Solar radiation	1 W/m^2	5% of full scale
Ultraviolet (UV) index	0.1	5%

Source: Davis Instruments, 2014.

Visual Assessment

Routinely, the exposed specimens were visually evaluated for damage. This was performed by comparing the specimens to earlier images and comparing different specimen locations (top vs. bottom, directly exposed area vs. area under a hold-down, etc.). Images were captured at different times to aid in determining if the sample conditions had changed.

Ground Penetrating Radar (GPR)

GPR works by sending an electromagnetic pulse into the target object and by receiving the reflected waves to characterize the contents of the object. Materials with different dielectric constants can be differentiated. Theoretically, any moisture in the HCB interior could be detected by GPR, since the dielectric constant for water is about 81 and for polyurethane and vinyl ester is approximately 3.0. Therefore, GPR was used to identify the presence of moisture within the FRP shell in a laboratory experiment. The inner foam surface of the bottom flange was applied with moisture at selected spots, and GPR was used to scan from the outer FRP shell surface to check for moisture detection. A GSSI StructureScan Mini XT device (Figure 9) was used for data collection, and GSSI's RADAN 7.0 software was used for data analysis.

Figure 9. Ground Penetrating Radar Device

Task 4: Evaluation of Deterioration

The deterioration of the HCB samples aged by accelerated laboratory exposure and environmental exposure was analyzed using SEM and XCT. These results were compared with values from tensile testing to failure.

RESULTS AND DISCUSSION

Task 1: Literature Review

One of the concerns with HCBs is the lack of a clear understanding of their structural behavior. Relatively few studies have attempted to explain the mechanism of load transfer and distribution in HCBs because of the novelty of this system (Aboelseoud and Myers, 2015; Ahsan, 2012; Harris and Civitillo, 2017; Van Nosdall et al., 2013).

Ahsan (2012) noted that most of the HCB components showed linear-elastic behavior under service level loads. However, in one of the trials, nonlinearity and small residual deflections were observed. Ahsan (2012) also observed that the concrete arch acted separately from the overall HCB behavior and was susceptible to local effects from loading. Local bending occurred in the arch, resulting in strains in excess of the cracking limit of concrete. This study also found that correction for skew was not included in the original Hillman model and that the model did not predict the behavior of the arch (Ahsan, 2012).

Van Nosdall et al. (2013) determined that the flexural rigidity of the tied arch component was about 80% that of the entire beam. On a related note, during noncomposite testing, the tied arch system carried 80% of the load and the FRP shell carried about 20% of the load. The study confirmed that the transformed area method was useful for the FRP shell and tension ties but did not work well for the arch. However, for the composite condition, the concrete arch was found to make a minimal contribution to the HCB stiffness and strength because the majority of the arch was below the neutral axis. The arch also cracked under the maximum live load. At this condition, the FRP shell and tension strands carried about 80% of the applied load and the deck carried most of the remaining loads (Van Nosdall et al., 2013).

A study by Aboelseound and Myers (2015) involved finite element modeling of HCB bridges. The studied concluded that the transformed area method was significantly conservative in predicting the deflection of HCBs. The numerical simulation predicted that the maximum deflection caused by the AASHTO notional loads was approximately 17% of the permissible live load deflection. The finite element model predicted lower stresses carried by the FRP shell under service loads, which could allow the FRP shell to have a high durability and thus could increase the service life of HCBs.

A field instrumentation of an HCB bridge in Virginia by Harris and Civitillo (2017) confirmed the location of the neutral axis above or near the top of the concrete arch once the beams became composite with the deck.

Durability

Another concern is that the durability of the entire HCB system depends on the outer shell. If the shell degrades because of environmental exposure, such as to salt spray or UV rays, or if the shell is damaged, such as by vehicle collision, then the integrity of the beam may be compromised. Thus, the durability of the outer shell needs to be studied. In addition, the success with which the outer shell can resist the penetration of moisture also needs to be studied. If moisture or contaminants can diffuse through the shell, even at a slow rate, the embedded tension reinforcement may start to corrode. The filler foam, being a closed cell polymer material, will not hold moisture; however, the moisture can stagnate in the bottom and increase the probability of corrosion. In addition, the moisture could collect between the shell and the foam or the concrete and the foam.

As per the study by Van Nosdall et al. (2013), in a composite design condition when the beams are in service, the FRP shell and tension strands carry about 80% of the loads. This highlights the significant role the FRP shell plays regarding the integrity of the HCB, beyond serving as a water-resistant box. This led the authors to concentrate on the durability of the FRP shell.

Vinyl Ester Resin

Vinyl ester resin is an organic thermosetting resin, used in FRP-matrix composite materials. Vinyl ester resin, although more expensive than polyester resin for similar purposes, has considerable commercial interest in boat manufacturing because of the higher resistance to degradation by corrosive and hostile environments (Telang et al., 2006, Visco et al., 2012).

Visco et al. (2012) tested the influence of exposure to seawater on the mechanical properties of various resin materials. Vinyl ester resin showed the highest resistance to the seawater degradation after accelerated aging tests of undercured matrices, which was verified using various evaluation methods such as calorimetric analysis, FTIR, SEM, contact angle measurement using the sessile drop technique, density measurements, Vickers hardness, and Izod resilience. The degradation of vinyl ester resin occurred mainly by surface hydrolysis, where the water was observed to detach surface layers of material rather than penetrate or diffuse into the matrix network.

Signor et al. (2003) exposed vinyl ester resin to artificial UV radiation for up to 4,000 hr. The ultimate tensile strains for 0 hr; 1,000 hr; and 4,000 hr of UV exposure were 16.72%, 14.98% (~10% decrease from 0 hr), and 8.92% (~46% decrease from 0 hr), respectively; the average specific toughness values were 1.44, 1.26 (~12% decrease from 0 hr), and 0.56 kg mm/mm^2 (~61% decrease from 0 hr), respectively. The average modulus of elasticity, however, increased with UV exposure at 1,000 hr but remained at the same range at 4,000 hr. This indicated an initial growth in brittleness, which would be expected with UV exposure. X-ray photoelectron spectroscopy showed surface degradation at the outermost thin layer with an increase in oxygen concentration. Signor et al. also reported that the FTIR-attenuated total reflectance probe's depth of penetration was limited to the top 3 to 5 μm (~0.1 to 0.2 mil).

Inspection

From the point of view of bridge owners, an even more important concern is the reliable inspection of HCBs. NCHRP Report 564 contains guidance for inspection of FRP bridge decks, where the main methods prescribed are visual inspection and tap testing that is analogous to chain dragging (Telang et al., 2006). However, the authors warned that tap testing or any sounding technique could be very misleading because of the stiffeners and other unexpected geometry of the FRP material. The study (Telang et al., 2006) also lists other nondestructive evaluation techniques, but they are essentially to detect delaminations and volumetric issues; none of the methods prescribed could detect or monitor the degradation of the FRP material.

The important structural members, concrete arch and tension ties, are hidden behind the FRP shell. Any degradation of the concrete and/or corrosion in tension strands may remain concealed until the damage has propagated severely. In addition, given the importance of the FRP shell to the durability of the HCB, no clear way exists to inspect them other than visually. The main objective of this study was to find reliable ways to inspect HCBs and get an indication of the durability of the FRP shell.

Task 2: Laboratory Accelerated Exposure

Figures 10 through 12 show the laboratory specimens at 0 hr, 920 hr, and 2,000 hr of UV aging, respectively. Visually, the specimens appear to become darker. However, no damages such as pitting, cracking, or crumbling were observed except on Specimen 8, which developed a burn on the surface at 920 hr (Figure 11). This black spot can be observed to grow bigger at the end of 2,000 hr of UV aging (Figure 12). This might have been because of the presence of a thin delamination from the load testing at Virginia Tech. Based on this, there was a suspicion that the accelerated exposure might be too aggressive in the later stages of the degradation and might not represent the actual conditions of the field structures, so the aging was stopped at this stage.

FTIR

Figures 13 and 14 show the FTIR scans of typical laboratory and field exposure specimens, respectively. Qualitative observations of FTIR spectra for the accelerated exposure machine specimens revealed various levels of exposure or degradation; how the qualities of the spectra from laboratory exposure specimens may relate to the field specimens is discussed later. The attenuated total reflectance probe is surface sensitive and thus not a probe of bulk organic chemicals, since the evanescent wave probes into the surface only a bit less than 2 to 10 μm. This varies inversely with the wavenumber and frequency of the infrared light probe and proportionally with the wavelength.

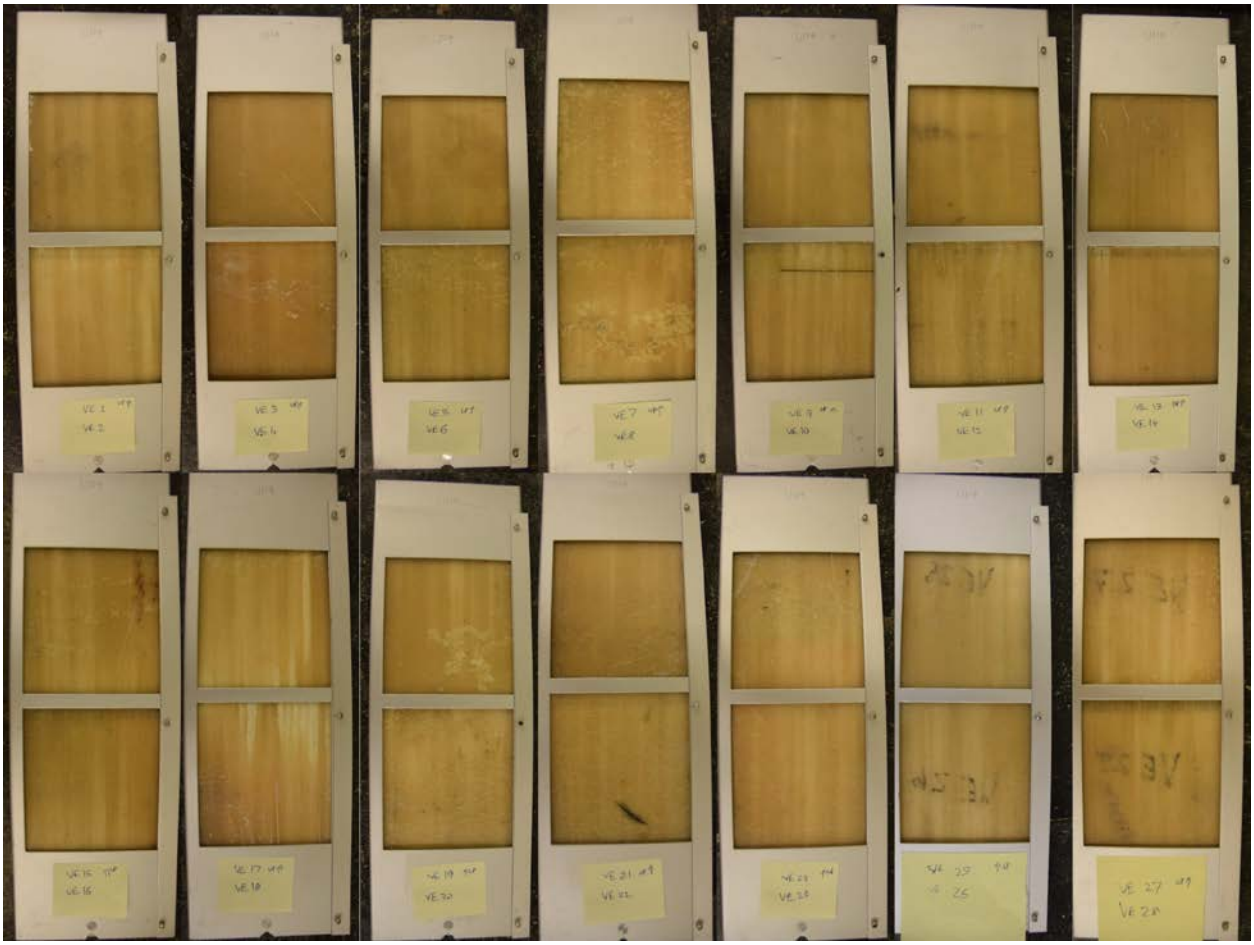

Figure 10. Laboratory Specimens at 0 Hours of Aging by Ultraviolet Radiation

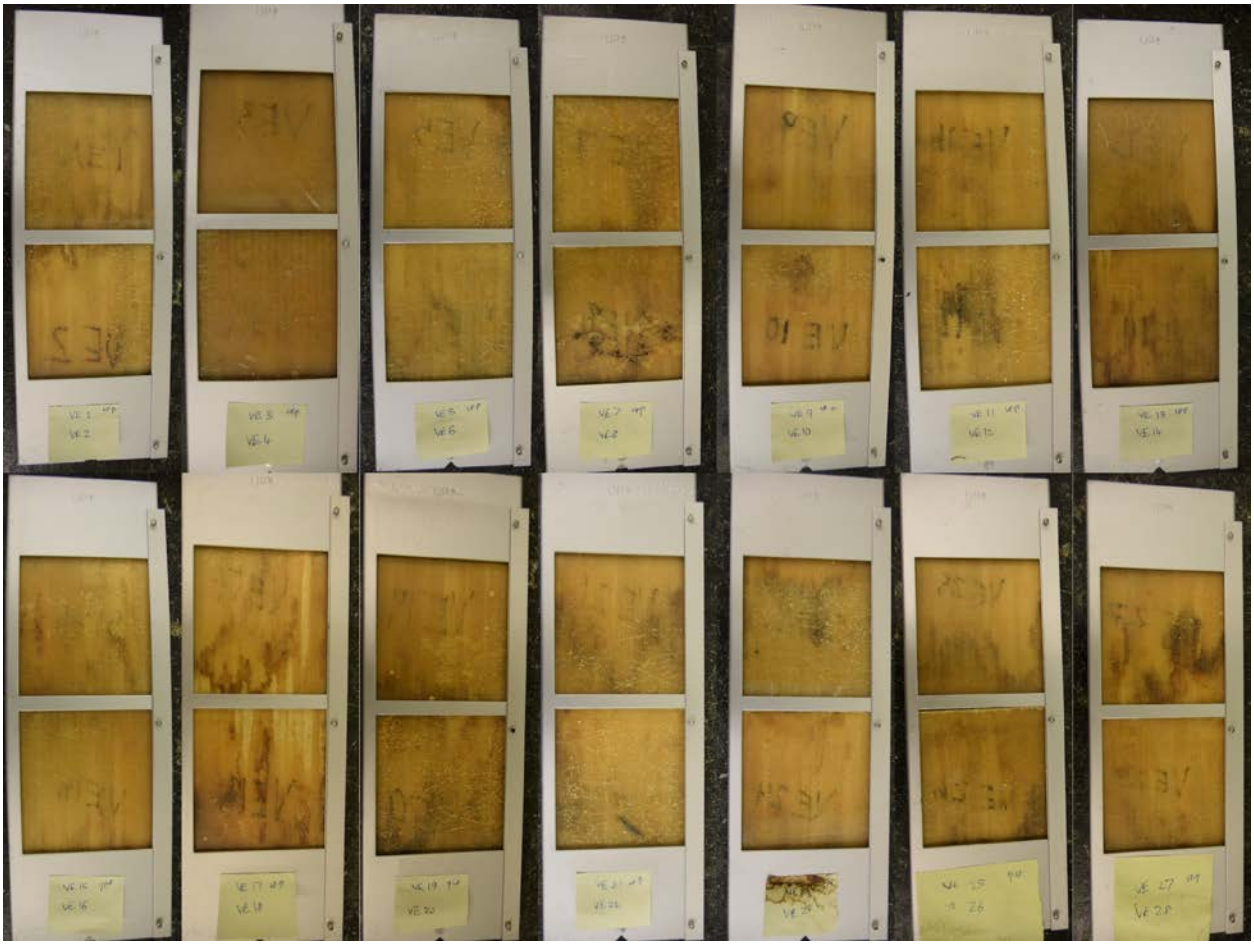

Figure 11. Laboratory Specimens at 920 Hours of Aging by Ultraviolet Radiation

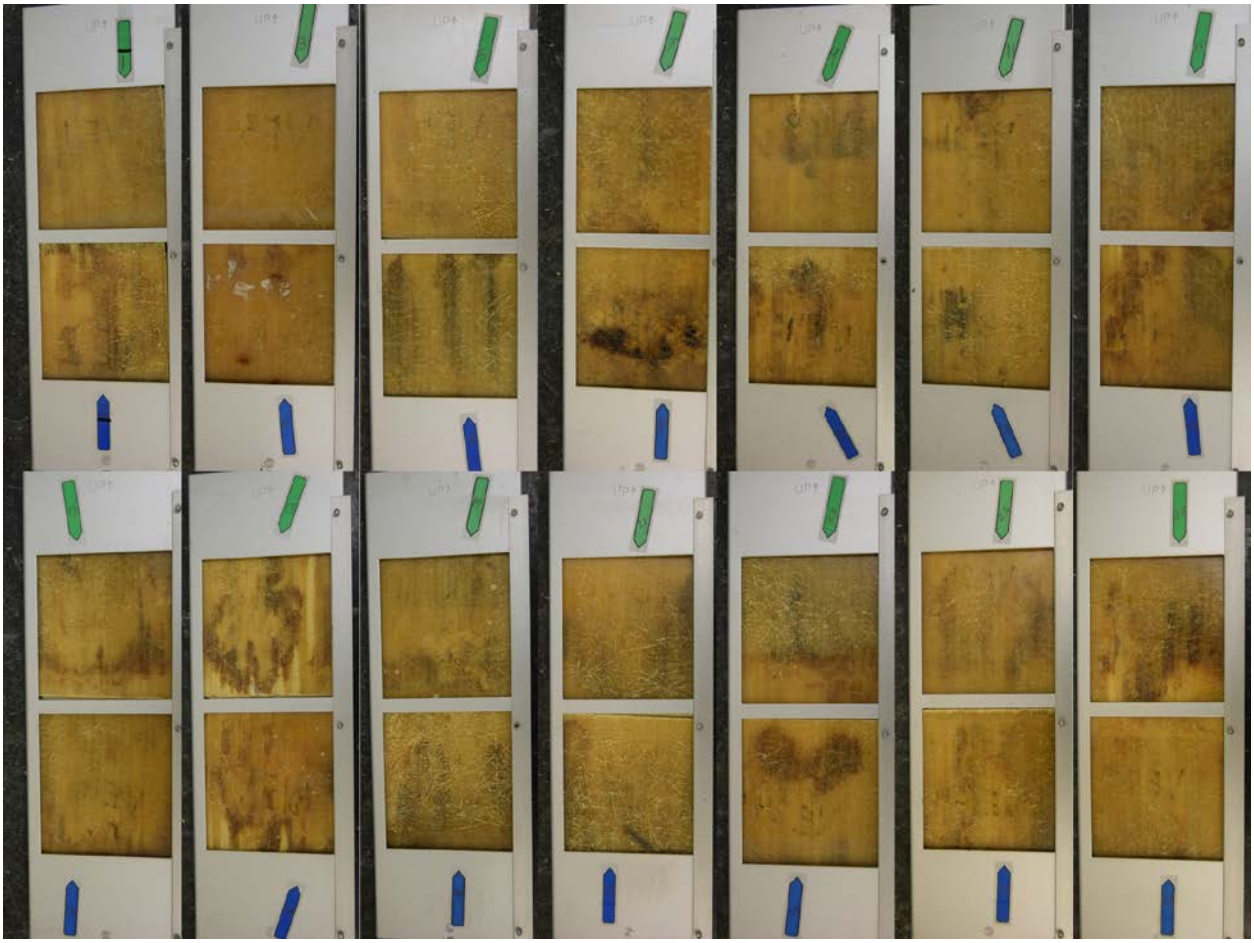

Figure 12. Laboratory Specimens at 2,000 Hours of Aging by Ultraviolet Radiation

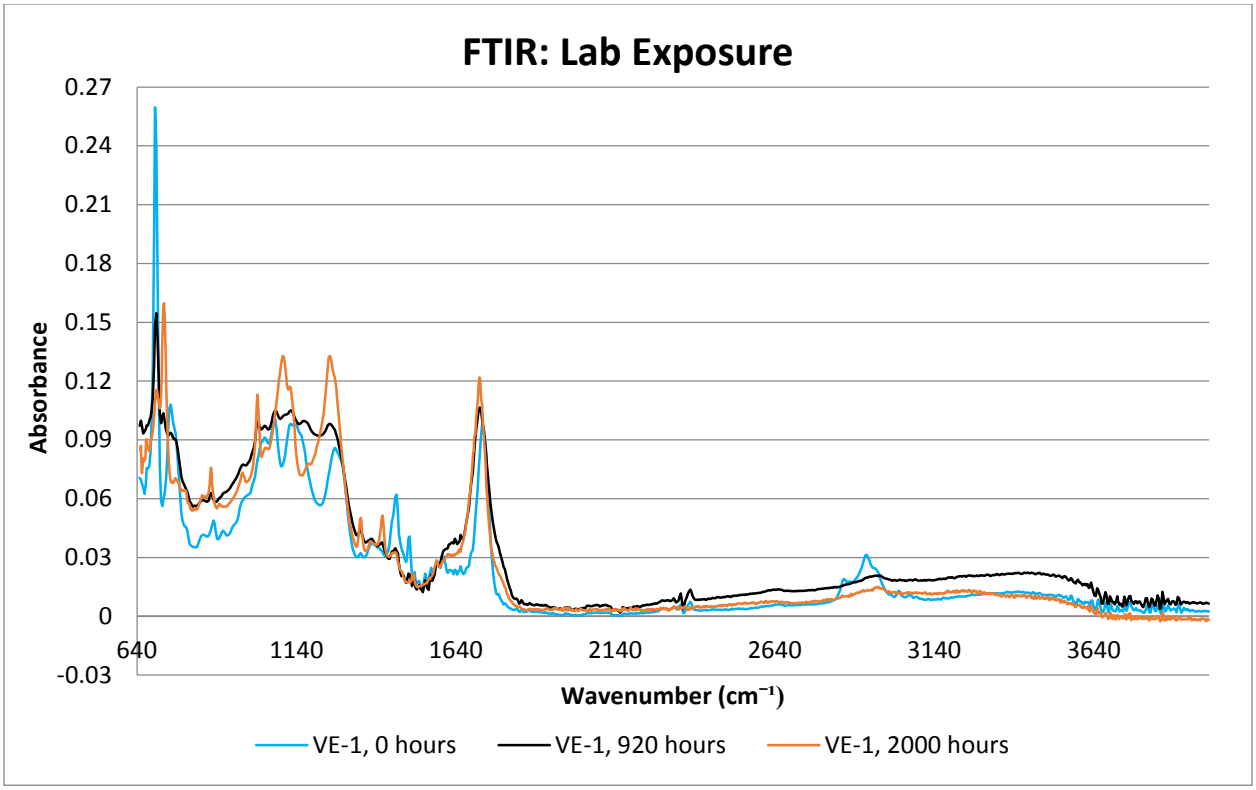

Figure 13. Fourier Transform Infrared Spectroscopy Scan of Laboratory Exposure Specimens

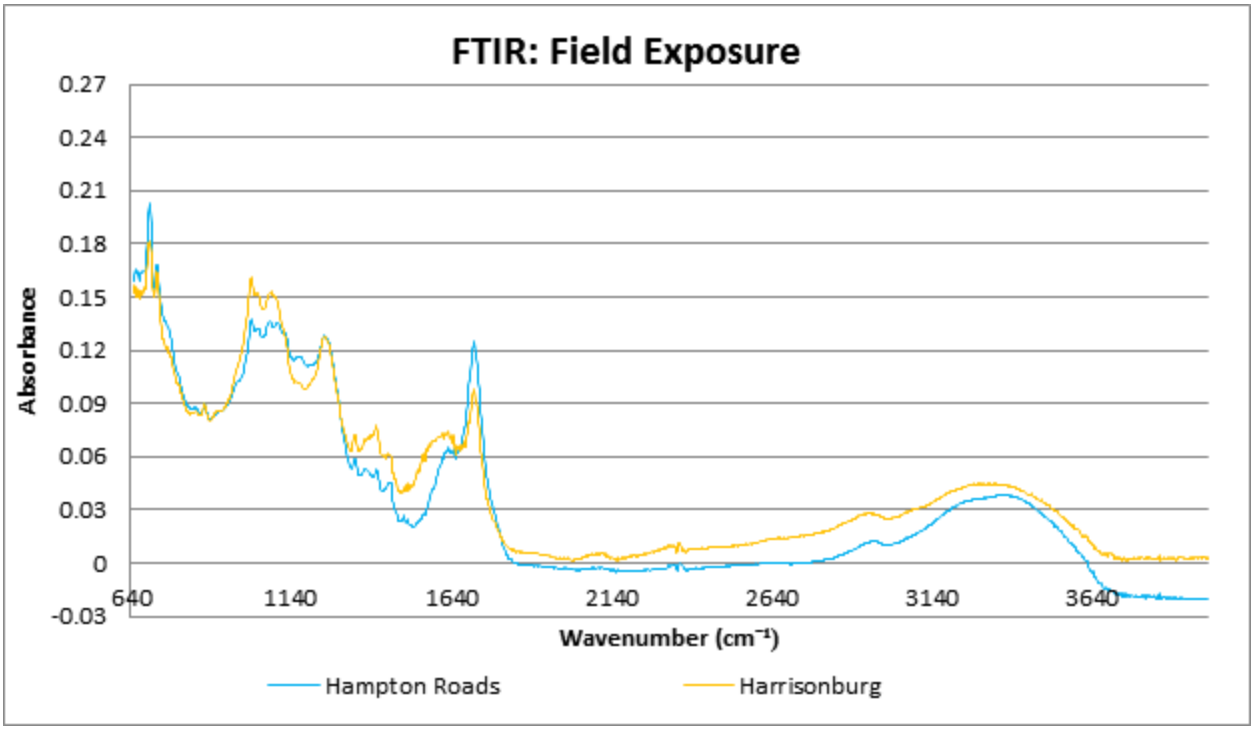

Figure 14. Fourier Transform Infrared Spectroscopy Scan of Field Exposure Specimens

Laboratory accelerated exposure specimens exhibited the following:

- A strongly absorbing peak around 700 cm^{-1} that appears to decrease in absorbance and eventually may be replaced with a peak around 725 cm^{-1}. Another nearby peak, initially present at 750 cm^{-1}, seems to disappear sooner than the 700 cm^{-1} peak.

- Minor peaks around 840, 870, and 960 cm^{-1} with the 870 cm^{-1} peak appearing to grow a bit faster than the others and simultaneously with the substantial decrease of a peak at 1160 cm^{-1}. A weak peak around 910 cm^{-1} also seems to disappear (possibly into the tails of nearby peaks).

- An increase in absorbance and a potential sharpening of 1100, 1120, 1250, and 1260 cm^{-1}, along with the growth of 1340, 1370, and 1410 cm^{-1} that is faster than 1450 cm^{-1}. In addition, the 1510 cm^{-1} peak appears to be quite weak, whereas 1605 cm^{-1} is observable.

- A prominent peak around 2925 cm^{-1} (wavenumber) for unexposed (nondegraded) specimens. This is in fact the strongest of a triple peak at 2850, 2925, and 2950 wavenumbers that is merely indicative of hydrocarbon content.

- A broad peak around 3400 cm^{-1} indicating increased hydrogen bonding. This hydrogen bonding could be because of one or more of at least a few changes: increase in water content, hydrolysis of ester linkage to produce carboxylic acids, and maybe others. Although hidden in this peak may be a narrower peak indicative of hydrogen bonding of alcohols, no clear conclusion could be drawn either way.

Field specimens exhibited the following:

- variable absorbance of 700, 725, and 750 cm^{-1}, with 700 and 725 cm^{-1} being the most prominent

- observable minor peak around 870 cm^{-1}

- strongly absorbing peaks at 1020, 1100, and 1245 to 1260 cm^{-1} and sometimes a weaker 1120 cm^{-1} peak, with a much weaker peak or near absence of a peak around 1160 cm^{-1}

- minor peaks around 1340, 1410, and 1450 cm^{-1} with just a bit of observable absorbance around 1510 cm^{-1}

- prominent 1610 cm^{-1} peak that would have to be deconvoluted from the 1725 cm^{-1} peak in order to be quantified

- a 2950 cm^{-1} peak that does not quite get lost in the tail of the 3400 cm^{-1} peak.

These molecular bond–level changes can be used as a benchmark against which further degradations can be chemically quantified in future studies, even though many of these observations do not mean much for the integrity of resin at present.

Around 1725 cm^{-1}, a shift toward lower wavenumbers of the carbonyl peak that is characteristic for esters (and carboxylic acids), as well as a weak increase in its absorbance with increasing exposure, was observed. The broadening of this peak did not appear to be monotonic, since the peak width first increased and then decreased with further exposure.

Thus, it appears that field specimens exhibit similar changes to exposure chamber specimens between 920 and 2,000 hr of exposure in the 1000 to 1300 cm^{-1} range (the "fingerprint" region). However the absorbance in the 700 to 800 cm^{-1} range and for both 2950 and 3400 cm^{-1} is stronger for field specimens when compared to that for the exposure chamber specimens of 920 and 2,000 hr. The higher absorbance for the 700 to 800 cm^{-1} range and 2950 cm^{-1} may possibly be because of higher hydrocarbon content near the surface of field specimens when compared with laboratory exposure specimens. The higher absorbance of the 3400 cm^{-1} peak may indicate either greater water content (from humidity) or hydrolysis of esters that has progressed further for field specimens in comparison to laboratory exposure specimens.

Colorimetry

Spectrocolorimeter readings were made on all laboratory specimens at the three stages. Results from the statistical analysis of the colorimetry values L*, a*, b*, C*, and h° are shown in Figures 15 through 19, respectively. An analysis of variance (ANOVA) was conducted for all parameters. The results are shown in tabular form at the top right of the images. The null hypothesis stated that the differences among the means of the three groups are not statistically significant. For all parameters (Figures 15 through 19), the p-value was less than 0.0001, which is less than the significance level (α) of 0.05, indicating that there were statistically significant differences between some or all of the groups: 0 hr, 920 hr, and 2,000 hr.

However, the actual differences among the groups cannot be found using this analysis. Therefore, a Tukey-Kramer test was conducted to understand the relative difference among the three sets of data.

Figure 15 shows the results for the L* (lightness) parameter. The plot shows the decreasing L* values with increasing duration of UV radiation exposure, almost in a linear fashion. The connecting letters report on the right side of the one-way analysis plot shows the results from the Tukey-Kramer test. The groups that are assigned the same letter are not significantly different, whereas the groups assigned different letters are significantly different. In this case, Figure 15 shows a big drop in lightness at 920 hr from 0 hr, but the drop was not statistically significant.

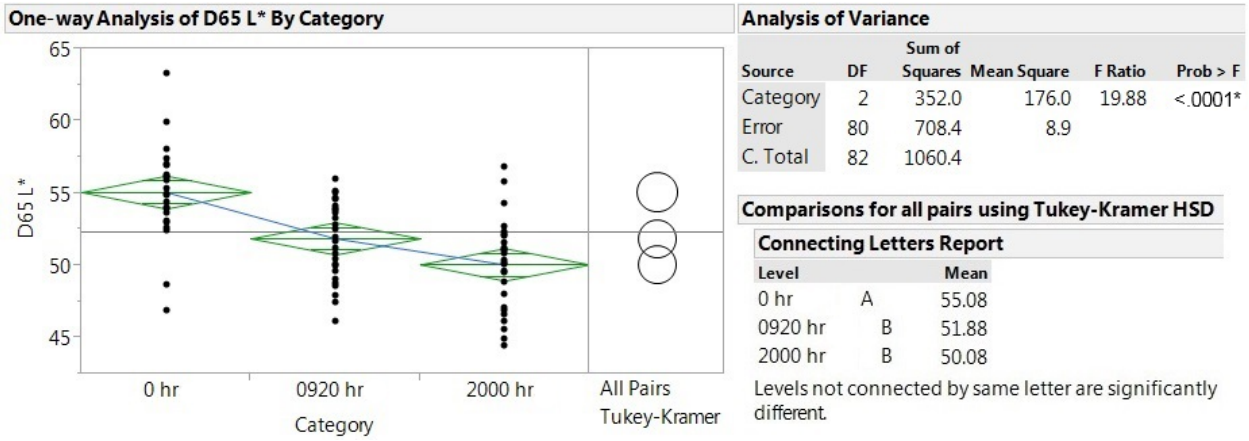

Figure 15. Statistical Means Comparison for D65 L* (Lightness) Values of Laboratory Specimens

Figure 16 shows the results for the a* (green-red) parameter. The plot shows increasing a* values with the increase in UV exposure, which is interpreted as an increase in the red component of the color. The connecting letters report from the Tukey-Kramer test shows that the increase in a* or red color was statistically significant with increasing UV exposure durations.

Figure 17 shows the results for the b* (blue-yellow) parameter. The plot shows increasing b* values with the increase in UV exposure up to 920 hr, which is interpreted as an increase in the yellow component of the color. No significant change was detected at 2,000 hr. The connecting letters report from the Tukey-Kramer test shows that the increase in +b* or yellow color was statistically significant at 920 hr from 0 hr but was not significant beyond that.

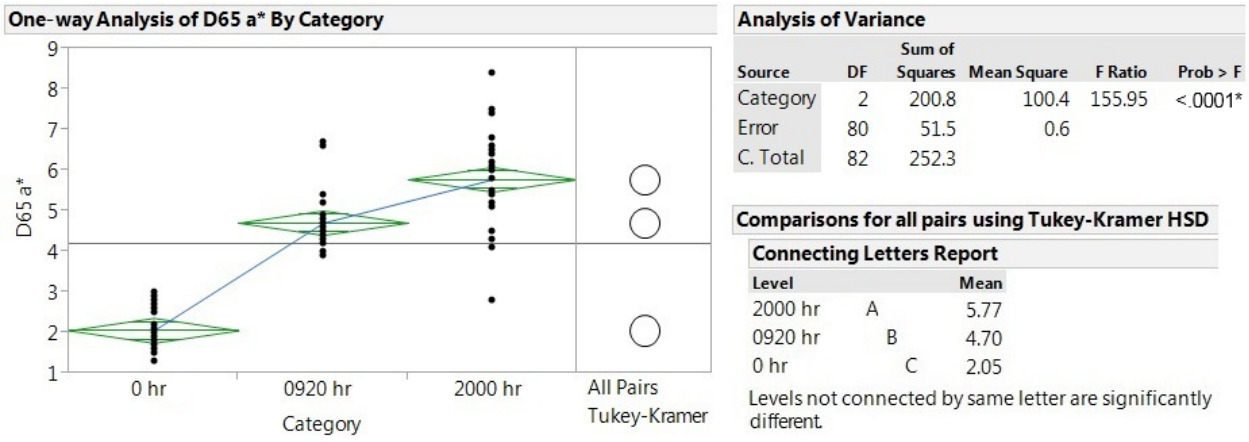

Figure 16. Statistical Means Comparison for D65 a* (Green-Red) Values of Laboratory Specimens

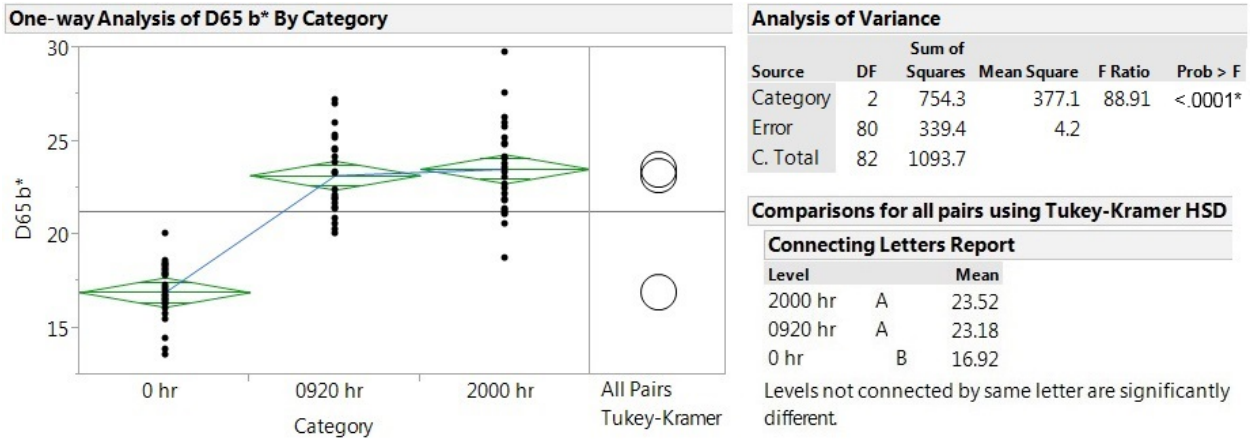

Figure 17. Statistical Means Comparison for D65 b* (Blue-Yellow) Values of Laboratory Specimens

Figure 18 shows the results for the C* (Chroma) parameter. The plot shows increasing C* values with the increase in UV exposure up to 920 hr, which is interpreted as an increase in the saturation or purity of the color. No significant change was found at 2,000 hr. The connecting letters report from the Tukey-Kramer test shows that the increase in C* was statistically significant at 920 hr from 0 hr but was not significant beyond that.

Figure 19 shows the results for the h° (hue) parameter. The plot shows the decreasing h° values with increasing duration of UV radiation exposure, almost in a linear fashion. This can be interpreted as the change in hue from near-yellow to brown as UV exposure increased. The connecting letters report from the Tukey-Kramer test shows that the increase in h° was statistically significant with increasing UV exposure duration.

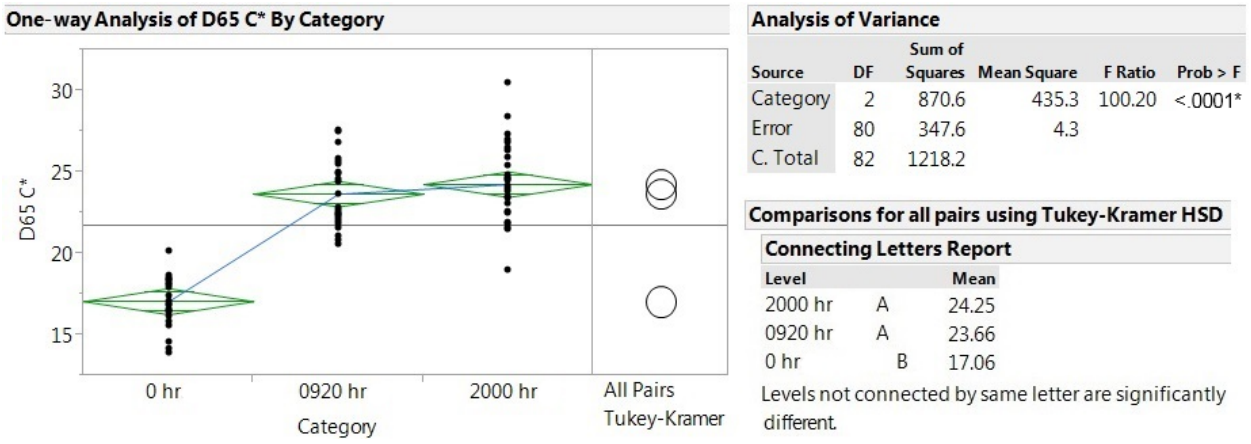

Figure 18. Statistical Means Comparison for D65 C* (Chroma) Values of Laboratory Specimens

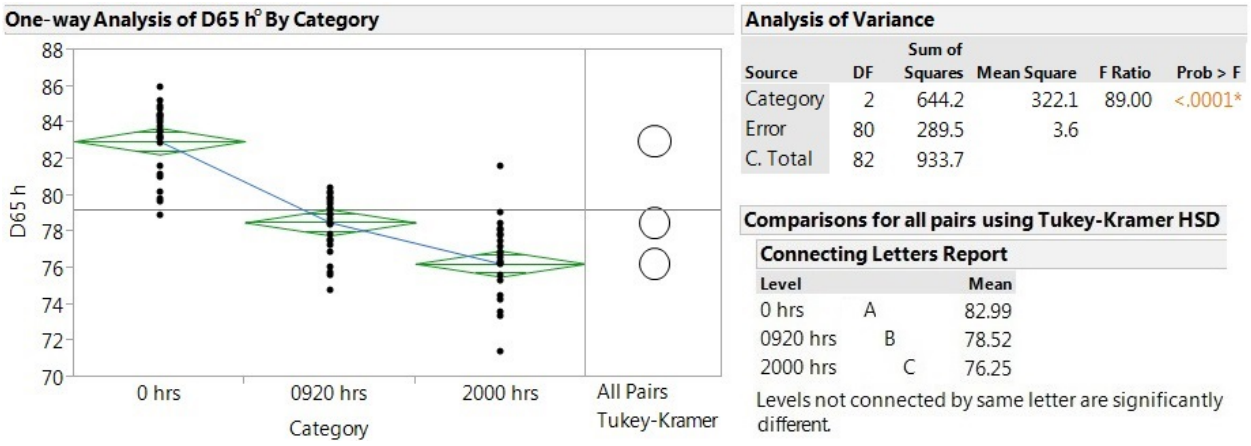

Figure 19. Statistical Means Comparison for D65 h° (Hue Angle) Values of Laboratory Specimens

From the results, it is understood that the colorimetry process provided a better understanding about the quantification of the color change, which can be easily missed by the human eye.

Spectrocolorimeter readings were made on two typical specimens from each of the field exposure sites at 1.7 years of exposure. It was observed during an attempt to measure colors during the daylight outdoors that excessive light could affect the measurements. This could be solved by using a simple light-blocking system around the spectrocolorimeter. However, in this study, the selected specimens were brought back to the laboratory to measure the color, since this environment had controlled background lighting.

Figures 20 through 24 show the results of the statistical analysis of L*, a*, b*, C*, and h°, respectively, from both laboratory and field exposure specimens. The L* values for the field specimens were significantly lower (darker) than that for the specimens exposed for 2,000 hr from the connecting letters report of the Tukey-Kramer analysis. This might appear as if the field specimens degraded more than the laboratory specimens with 2,000 hr of UV exposure. However, the color parameters cannot be evaluated individually. In addition, it should be noted that the laboratory accelerated exposure cycle involves condensation for 4 hr after the UV cycle, which will clean the surface of the specimens regularly. The field exposure specimens were exposed to sporadic precipitation and exposure to dust and other impurities, likely resulting in darker specimens. This can be concluded only by considering the other color-related parameters.

Figure 21 shows that the field specimens were lower on the a*, or red, scale and belong in the same level as the specimens that were never exposed and were significantly different from the exposed specimens. In addition, Figure 22 shows that the field specimens were lower on the b*, or yellow, scale and the same level as the specimens that were never exposed and were significantly different from the exposed specimens. Similarly, as shown in Figure 23, the field specimens were noted to have low Chroma values, significantly lower than the laboratory specimens exposed to UV radiation. Likewise, the hue angle was significantly lower than the exposed laboratory specimens.

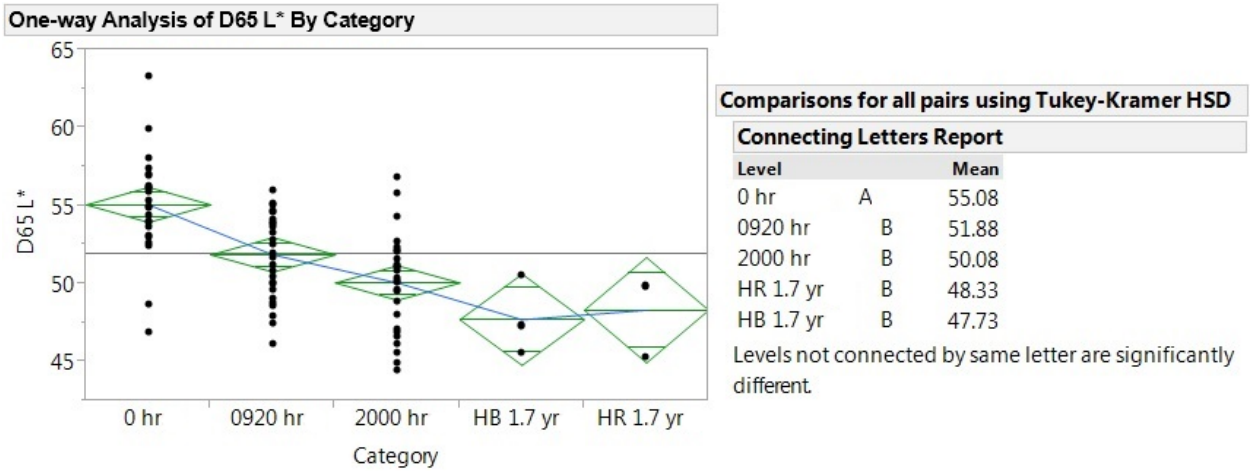

Figure 20. Statistical Means Comparison for D65 L* Values of Laboratory and Field Specimens

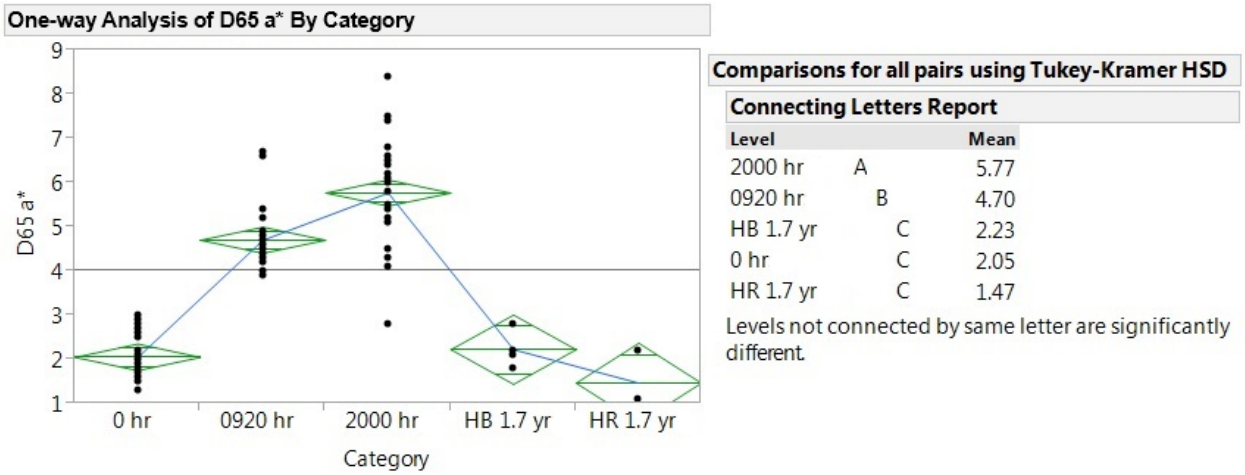

Figure 21. Statistical Means Comparison for D65 a* Values of Laboratory and Field Specimens

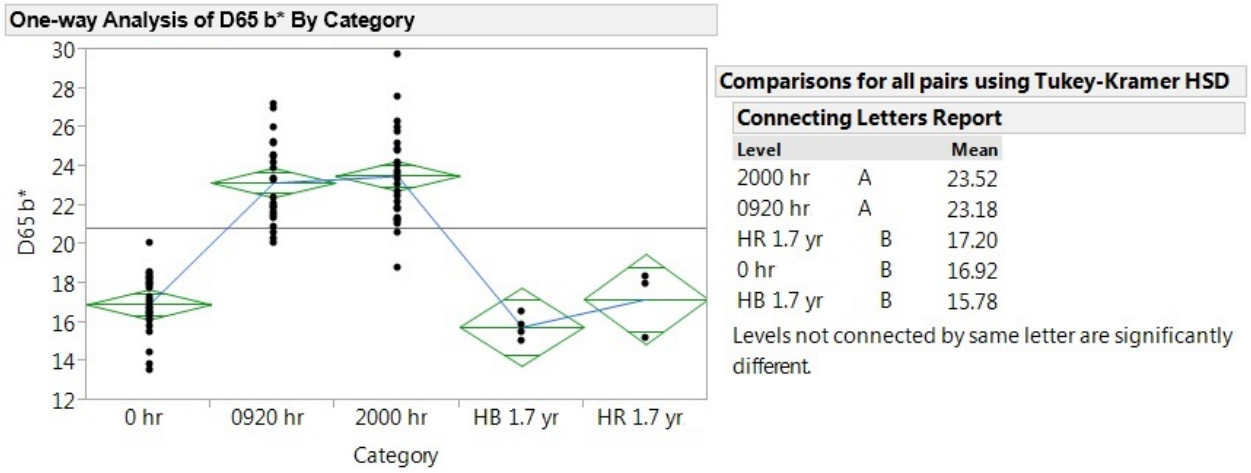

Figure 22. Statistical Means Comparison for D65 b* Values of Laboratory and Field Specimens

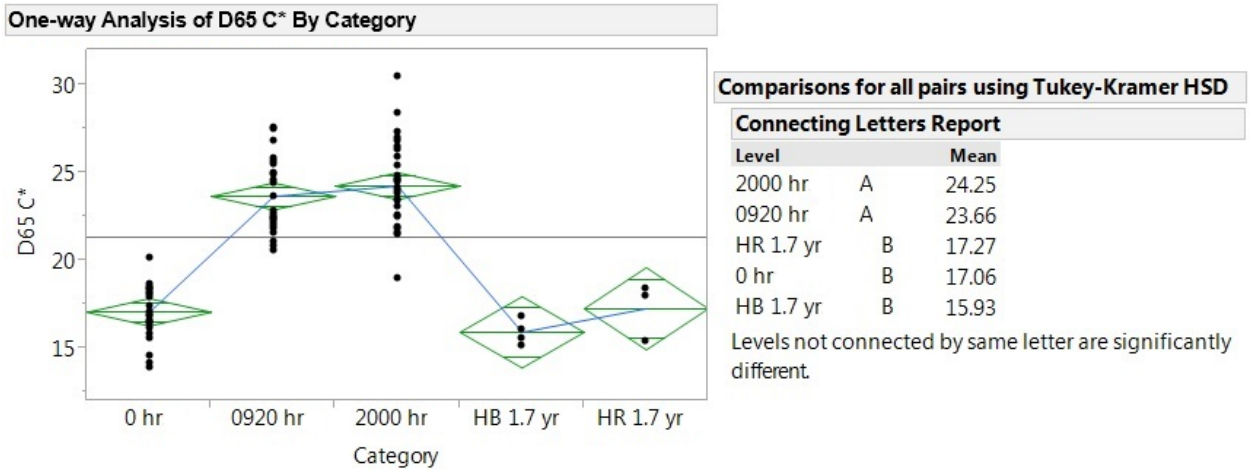

Figure 23. Statistical Means Comparison for D65 C* Values of Laboratory and Field Specimens

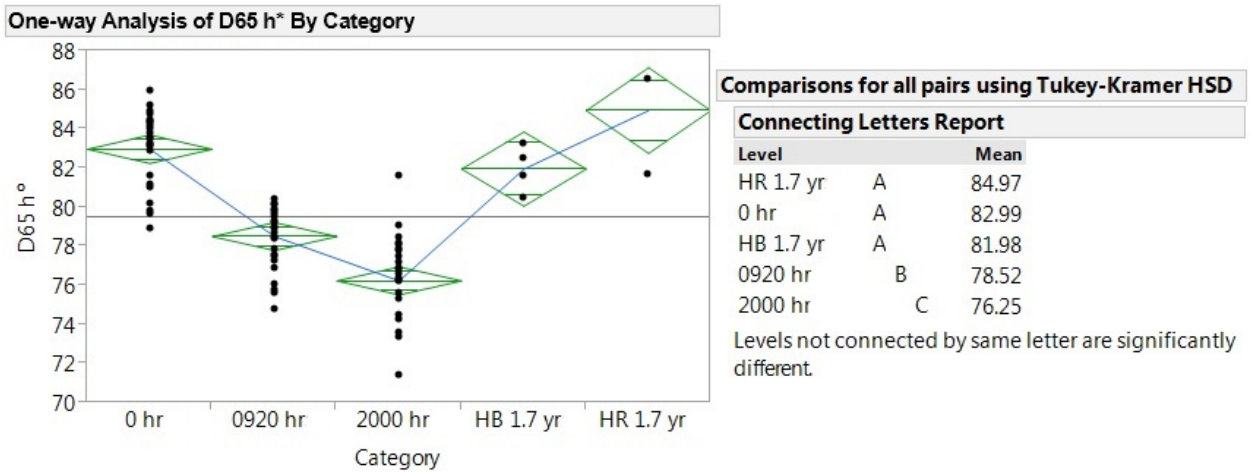

Figure 24. Statistical Means Comparison for D65 h° Values of Laboratory and Field Specimens

Thus, the results from the statistical analysis showed that the field specimens at 1.7 years of exposure did not reach the level of changes observed in the accelerated exposure specimens in the laboratory.

GPR

One of the primary indications of deterioration in the HCB is moisture leakage into the beam interior. This would point to breaches in the FRP shell and will eventually cause corrosion initiation in the steel strands, thus leading to the premature failure of its structural system.

An initial attempt was made on an HCB bottom flange slab to detect moisture, similar to the slab shown in Figure 1a, to calibrate the device. It is difficult to calculate the dielectric constants for a complicated structural member with layers of glass fiber–reinforced vinyl ester resin and polyurethane foam. Therefore, the dielectric constant was experimentally found as slightly less than 2.0, using known depth and time of flight. Since the equipment can be set only to a minimum dielectric constant of 2.0, it was set that way. The depth of features seen on the scans will be slightly deeper than they appear.

Figure 25 shows a GPR scan in the longitudinal direction of the HCB in the middle. The x-axis shows the longitudinal spatial length of the scan, and the y-axis shows the depth. Then, moisture was applied using a brush on the same section for a 12-in length from the edge. Figure 26 shows the GPR scan with the 12-in-long moisture signature clearly. It can be noted that the edge effect in the form of hyperbolas appears more prominent than the presence of water.

To test the sensitivity of GPR in detecting moisture, three circles of moisture of different sizes were dabbed using a brush at three locations along the same longitudinal section: 5-in, 1-in, and 4-in diameter from the left. Figure 27 shows the results from this scan. The locations of the water locations, even the one as small as 1 in, are clearly visible except that the first location from the left (5 in) was partly hidden by the edge effect.

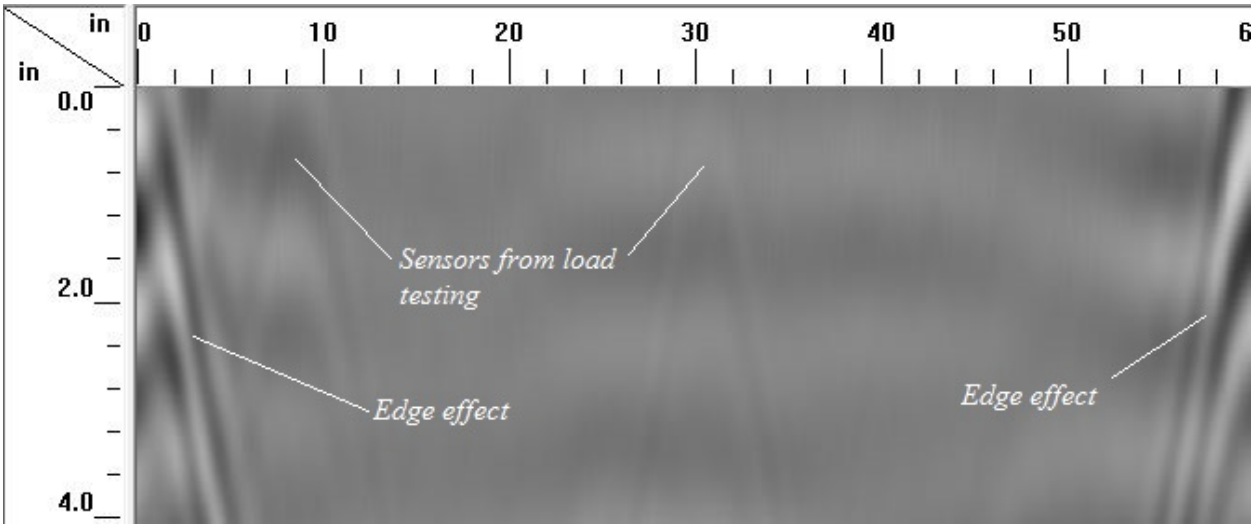

Figure 25. Ground Penetrating Radar Scan of Bottom Flange With No Moisture

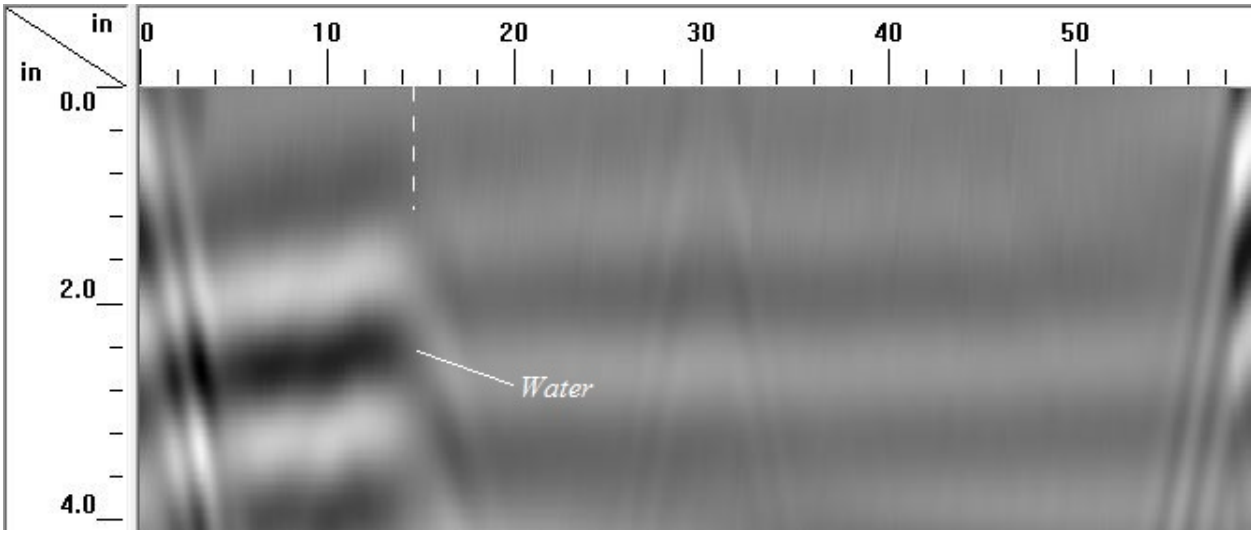

Figure 26. Ground Penetrating Radar Scan of Bottom Flange With Moisture

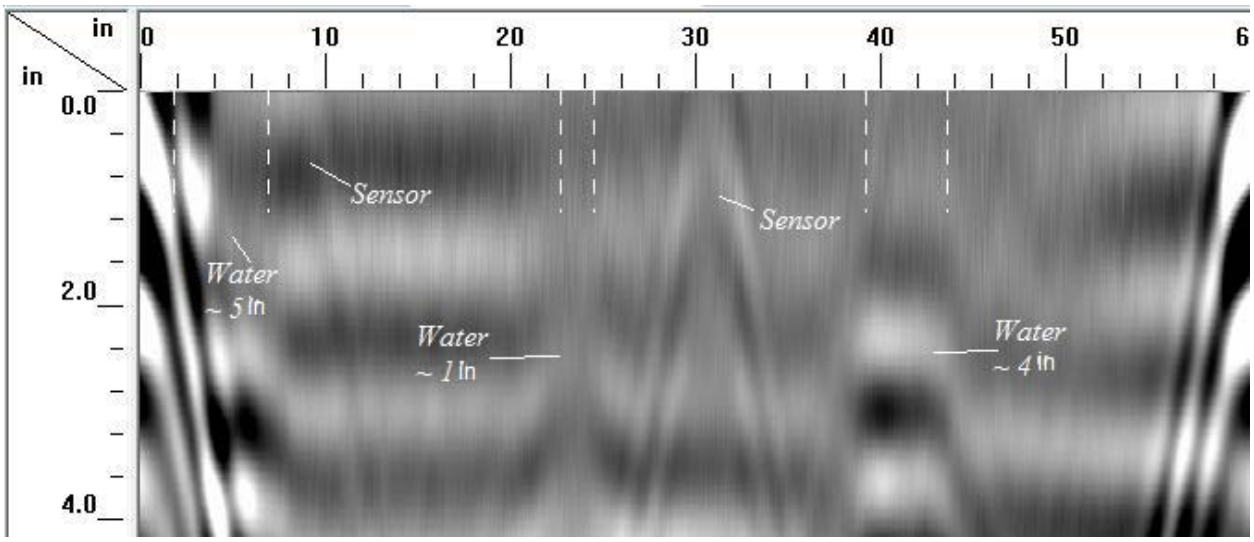

Figure 27. Ground Penetrating Radar Scan of Bottom Flange With Three Moisture Locations

This laboratory experimentation proves GPR's capability to detect even a trivial moisture presence inside the HCB.

Task 3: Field Exposure

Weather Data

The weather data collected exhibited the expected seasonal trends. Figure 28 shows the temperature behavior at both sites. Clearly, the temperature is warmest at both sites in the summer and coldest during the winter. The Harrisonburg site showed more extreme temperatures as compared to the Hampton Roads site.

This was also observed with the relative humidity measurements (Figure 29), with Harrisonburg showing a greater range but both sites having a similar maximum value.

Finally, Harrisonburg also showed the greatest amount of precipitation (Figure 30), but clearly both regions routinely received precipitation throughout the year.

If these were the only variables measured, it would appear that the Harrisonburg site might have represented more aggressive testing of the materials listed in Table 1. However, upon a review of the solar radiation (Figure 31) and UV index (Figure 32) data, the maximum solar radiation exposure occurred at the Harrisonburg site but the maximum UV index was recorded at the Hampton Roads site. These trends were considered as each exposed sample was visually evaluated, which is discussed later.

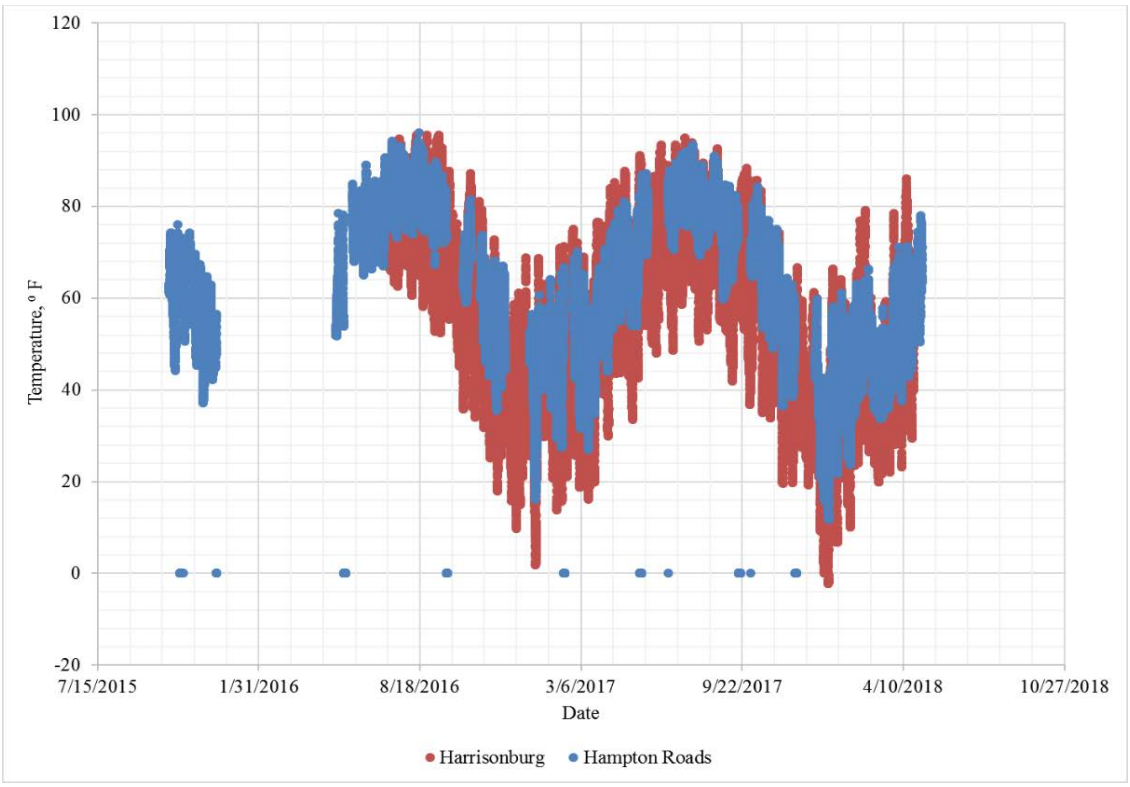

Figure 28. Temperature at Exposure Sites

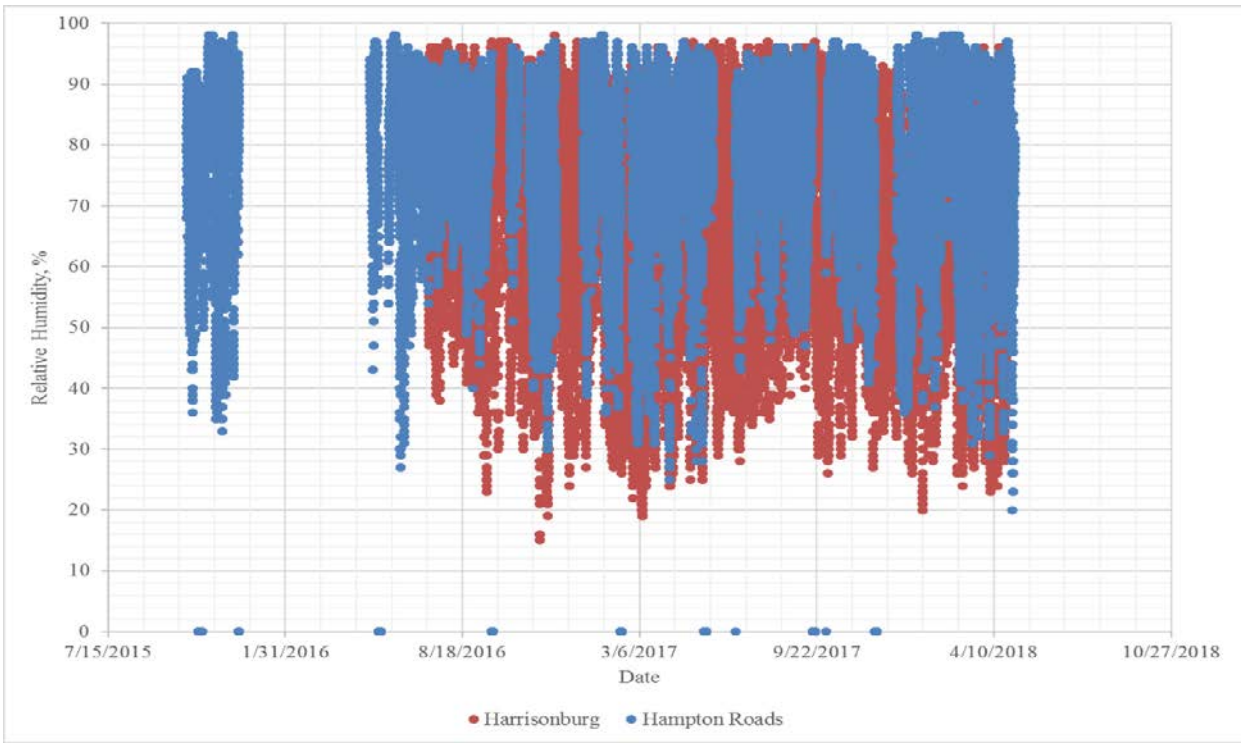

Figure 29. Relative Humidity at Exposure Sites

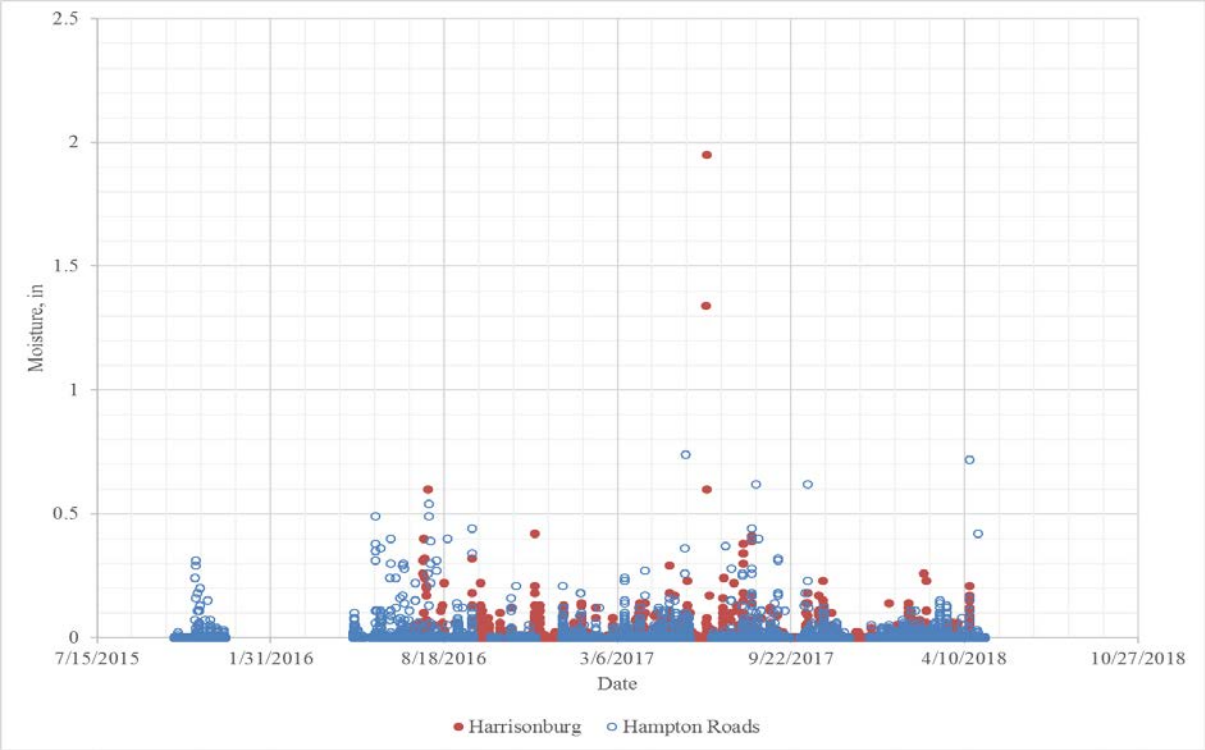

Figure 30. Precipitation at Exposure Sites

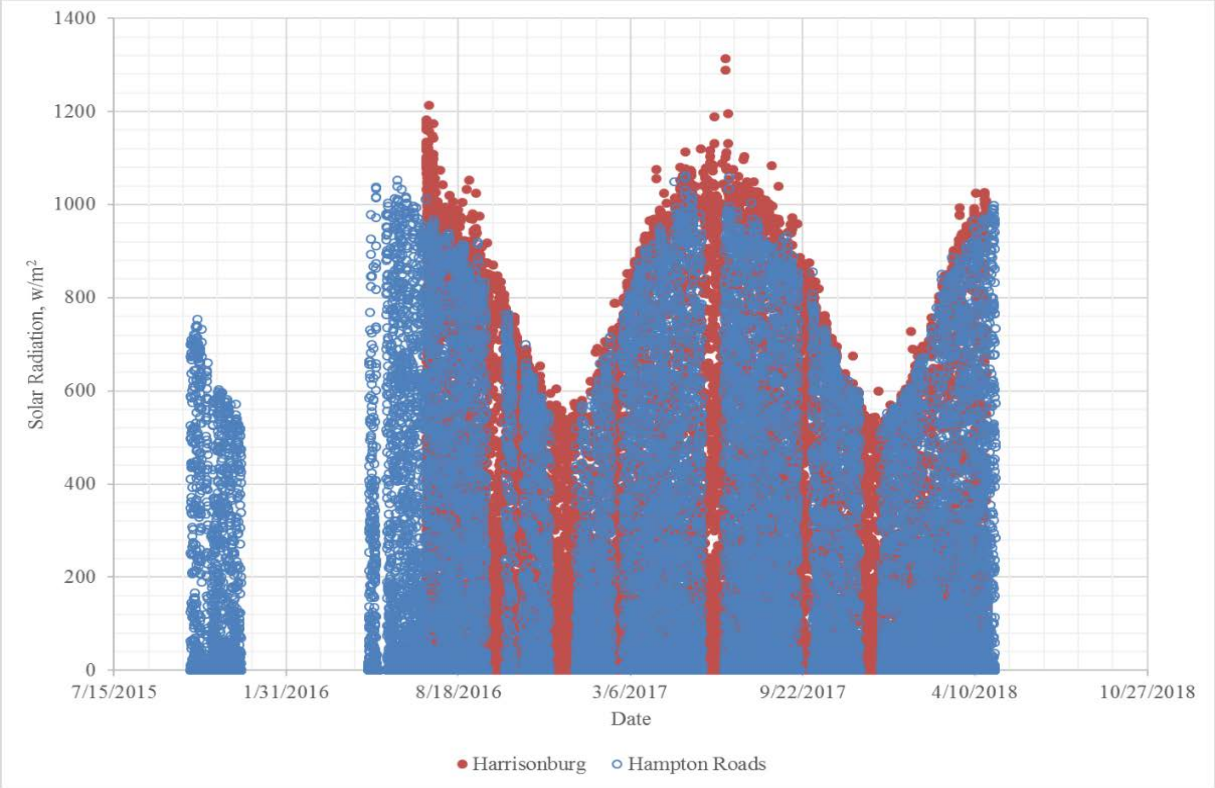

Figure 31. Solar Radiation at Exposure Sites

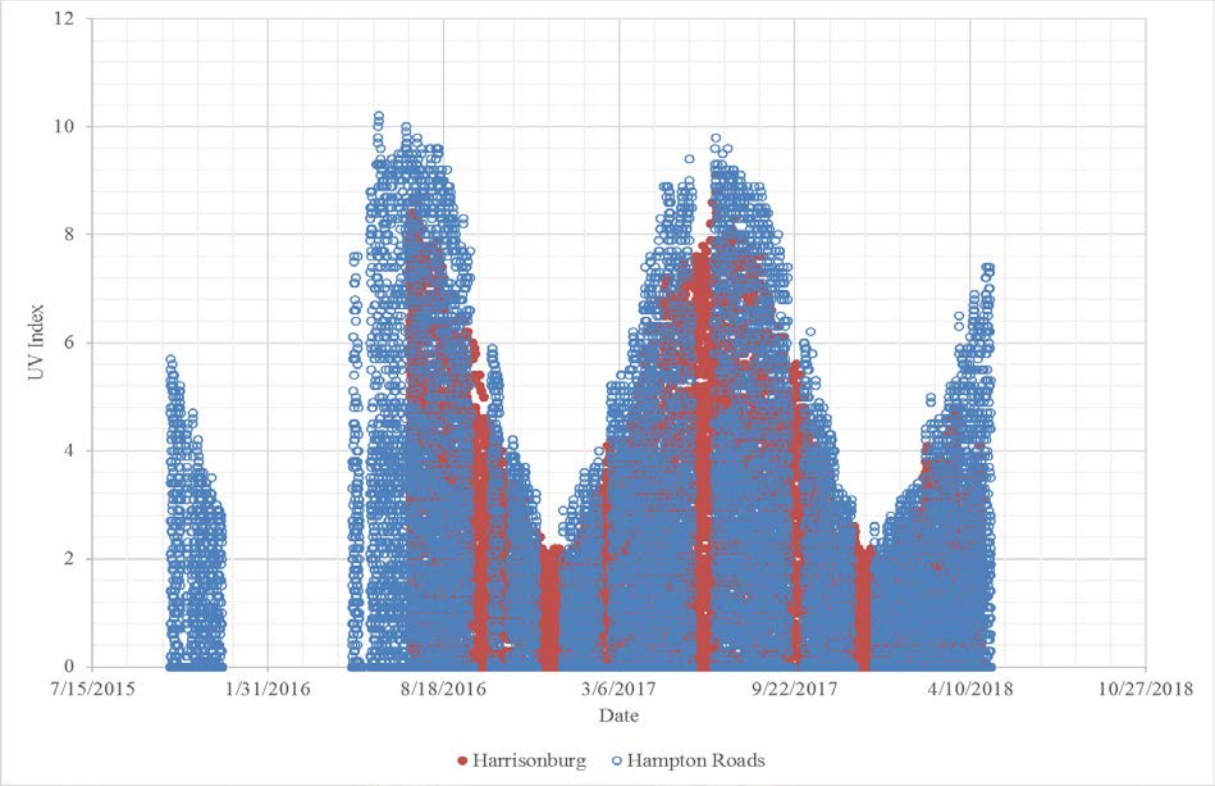

Figure 32. Ultraviolet Index at Exposure Sites

Visual Assessment

Harrisonburg Site

After 1 year and 8 months of exposure at the Harrisonburg site, the specimens showed some minor deterioration. Figures 33 through 35 show the initial condition of the specimens and then again after 1 year and 8 months.

Delamination of the glass layer was observed along a cut edge (Figure 33) in one sample, which was probably attributable to moisture penetrating the sample and expanding and contracting during seasonal cycles of freezing and thawing. Most of the specimens, however, visually seemed to have performed well and did not show signs of substantial degradation. This response was especially surprising for the foam specimens (Figure 35) since this component of the composite beam was somewhat protected from the weather because it was placed inside the fiberglass shell that makes up the beam.

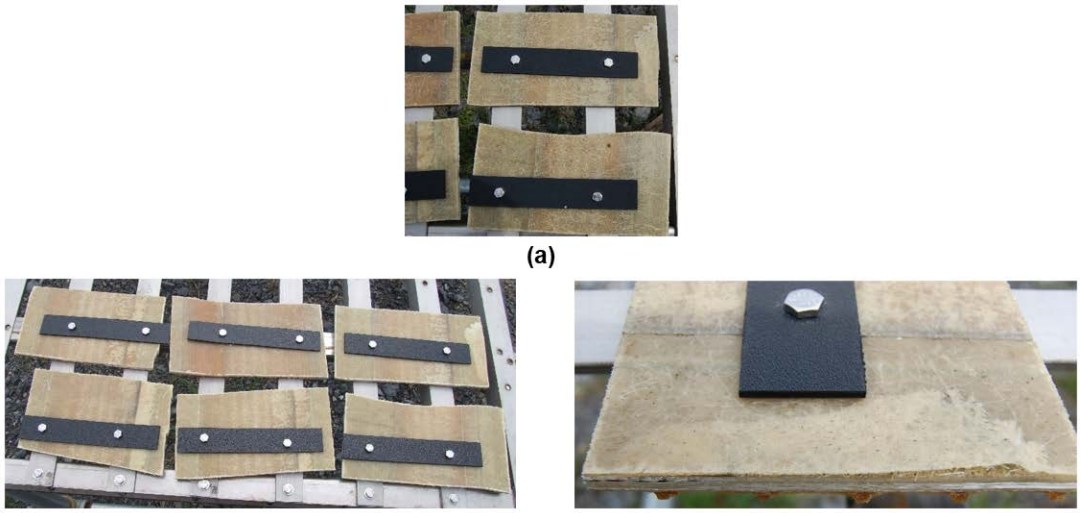

Figure 33. Comparisons of Fiberglass Specimens: (a) initially; (b) several specimens after 1 year and 8 months; (c) close-up of delaminated edge after 1 year and 8 months

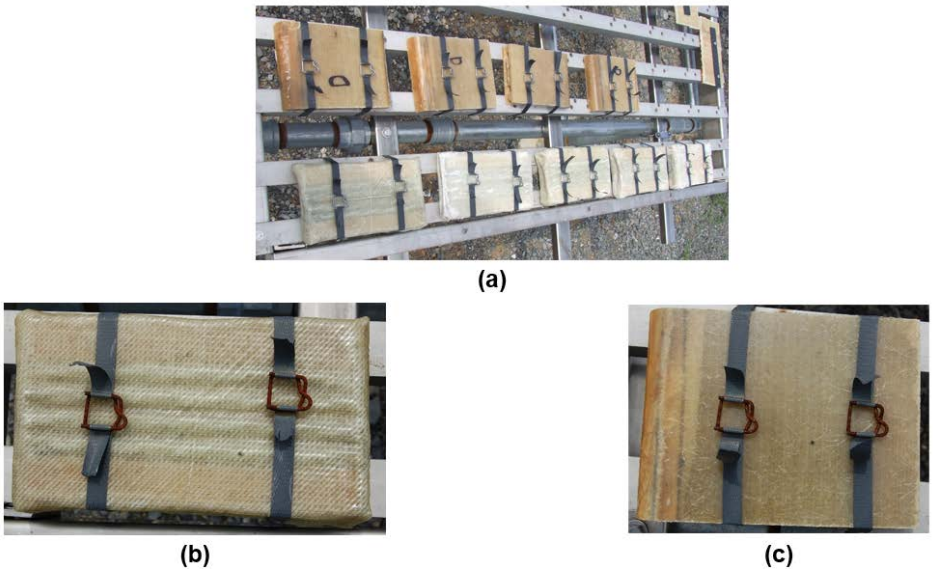

Figure 34. (a) Fiberglass with the exposed steel specimens, on upper sample line in each photograph, and fiberglass with the protected steel specimens shown along the lower sample line in each photograph with no exposure; (b) close-up of a typical protected steel sample after 1 year and 8 months; (c) close-up showing a typical exposed steel sample after 1 year and 8 months

(a) (b)

Figure 35. Comparisons of Foam Specimens: (a) initially; (b) after 1 year and 8 months

Hampton Roads Site

After 1 year and 8 months of exposure at the Hampton Roads site, the sample showed some minor deterioration but the amount of damage was greater than that at the Harrisonburg site. Figures 36 through 38 show the initial condition of the specimens and then again after 1 year and 8 months.

Delaminations and damage to the exterior surface of the fiberglass layer were observed (Figure 36) in several specimens. Other test specimens that exhibited damage also included the foam, which clearly exhibited more damage, as seen in Figure 38. This was interesting since the weather data for this site were less extreme as compared to the Harrisonburg site with the exception of the UV index data. Therefore, it appears that although the composite beam components showed only minor deterioration, UV exposure most likely contributed the most to damaging the exposed components.

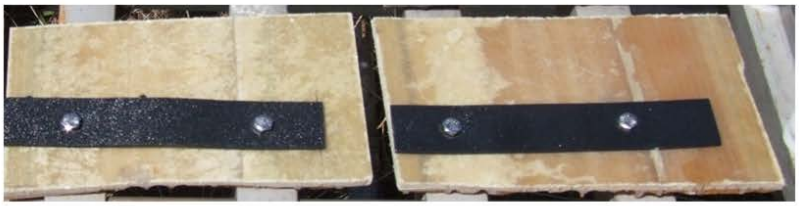

(a)

(b)

(c)

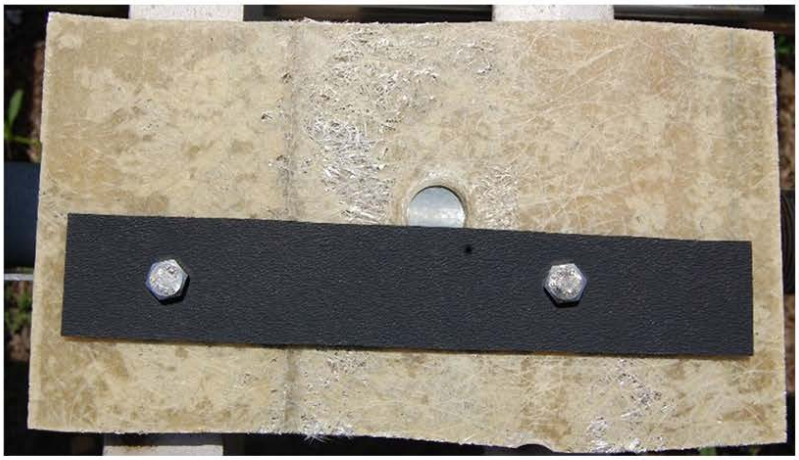

(d)

Figure 36. Comparisons of Fiberglass Specimens: (a) initially; (b) after 1 year and 8 months, exhibiting delamination and exposure of the fibers; (c) in an area that initially had some fibers showing; (d) observed to have grown larger after 1 year and 8 months

(a)

(b)

(c)

Figure 37. (a) Fiberglass with the exposed steel specimens, on upper sample line in each photograph, and fiberglass with the protected steel specimens shown along the lower sample line in each photograph initially; (b) close-up showing a typical protected steel sample after 1 year and 8 months; (c) close-up showing a typical exposed steel sample after 1 year and 8 months

(a) (b)

Figure 38. Comparisons of Foam Specimens: (a) initially; (b) after 1 year and 8 months showing how foam has degraded and exhibits loss of material, especially along the edge because of exposure

Task 4: Evaluation of Deterioration

Since Ahsan (2012) discovered that the FRP shell ended up carrying about 80% of the load, because of the concrete arch failure when made composite with the beam, the importance of fiber within the FRP has increased with regard to the structural integrity of HCBs.

The resin not only embeds the glass fibers to maintain the shape and pattern of reinforcement but also protects the fibers from exposure to the environment. Figure 36 shows that the resin could wear away under exposure from freeze-thaw cycles and other environmental factors. This can expose the embedded glass fibers that carry the entirety of tensile stress in the members. In addition, scraping against flotsam such as tree branches under the bridge can easily wear away the resin and a few layers of glass fibers. Since this type of deterioration is more likely to happen throughout the service life of the structure, rather than with a complete puncture, an investigation of scraping with the tensile strength of the material was carried out.

For this investigation, the placement and orientation of the fibers inside the resin must be identified. High-resolution optical imaging was performed on polished cross-sectional surfaces of specimens, as shown in Figure 39. Identifying fiber layers and orientation was difficult because of the uneven resin concentration and translucence of the material. Thus, better techniques were attempted to understand the sample composition.

Figure 39. High-Resolution Optical Imaging of Polished Fiber-Reinforced Polymer Specimen

SEM

This technique uses a scanning electron microscope to produce extremely high-resolution images of specimens. SEM focuses a beam of electrons on to the scanning surface. The electrons interact with the atoms and produce signals proportional to the topography of the sample surface. Resolution of the SEM can be from 1 to 20 nm (4×10^{-5} to 7.8×10^{-4} mils) depending on the instrument. Figure 40 shows an SEM image of the polished surface of the same sample from Figure 39. Although the SEM image provided more details and confirmations about fiber mat layers, it was still difficult to determine the fiber orientations.

A magnified portion of Figure 40 is shown in Figure 41. The fiber layers can be easily identified; however, as stated before, the fiber orientations appear vague. In the same image, the bottom surface of the sample shows some rough edges that were not polished well. It was ironically more useful in identifying the fiber strands and orientation. The rough clump of fibers runs perpendicular to the plane of the image, as indicated by the circular cross section of the individual fiber strands. It was found that unpolished specimens also provided less reliable visualization of the resin.

Therefore, further specimens were polished mildly, to remove dirt and foreign material, before SEM imaging was performed, as shown in Figure 42. However, the outer layer of FRP (top two-thirds thickness of Figure 42) showed irregular and scarce fiber content without a particular orientation. It is possible that there were fiber mats in this layer, but was not visible on the surface.

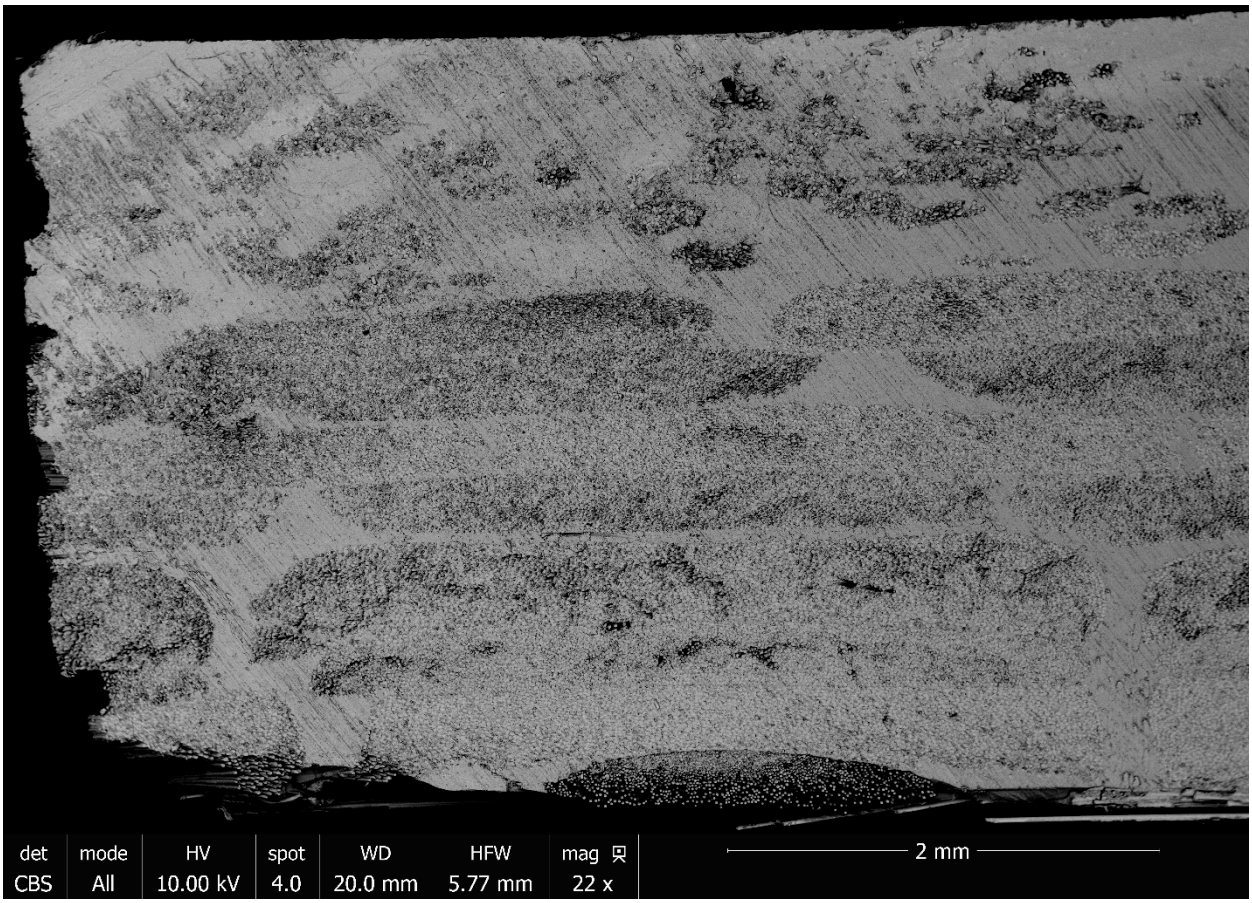

Figure 40. Scanning Electron Microscope Image of Highly Polished Fiber-Reinforced Polymer Sample

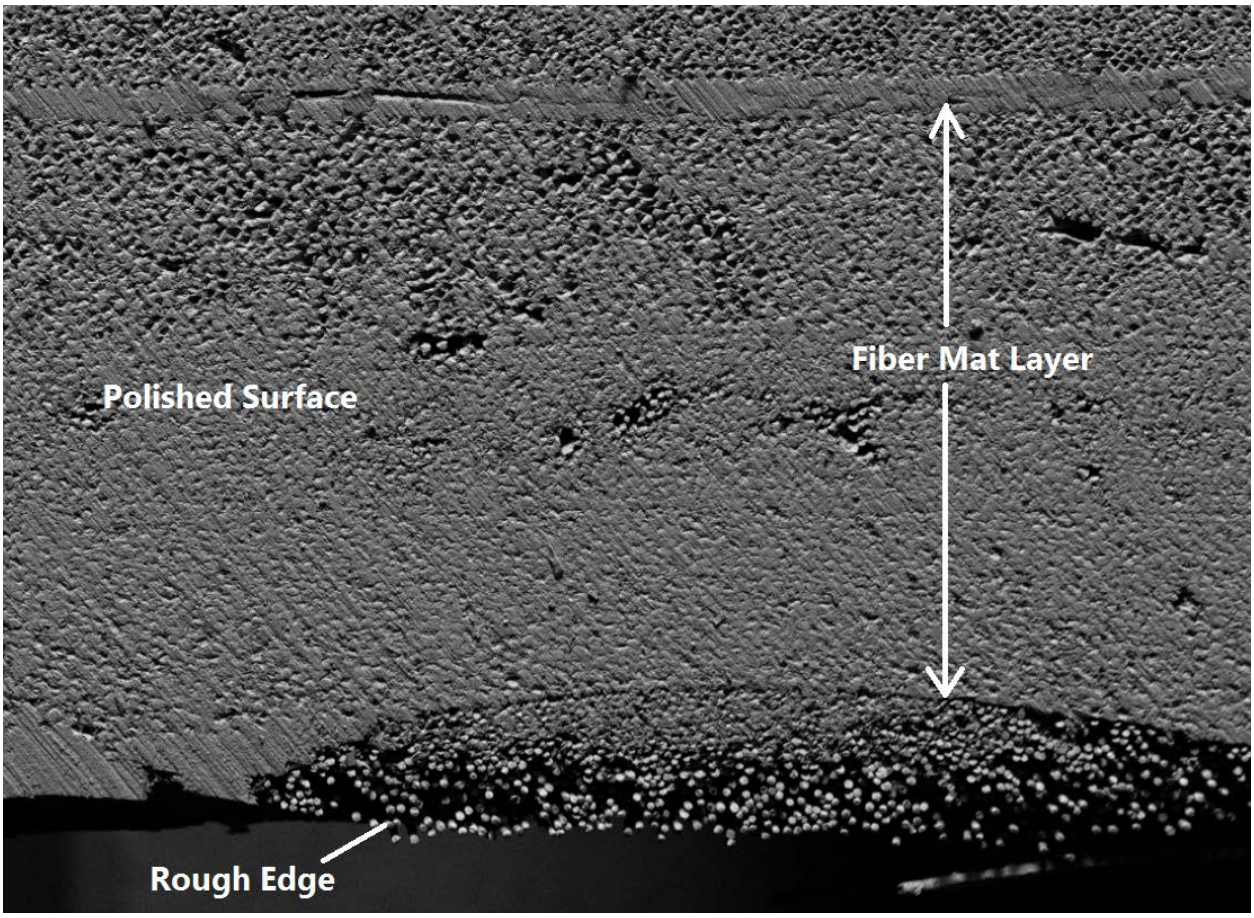

Figure 41. Magnified Scanning Electron Microscope Image of Polished and Rough Edges

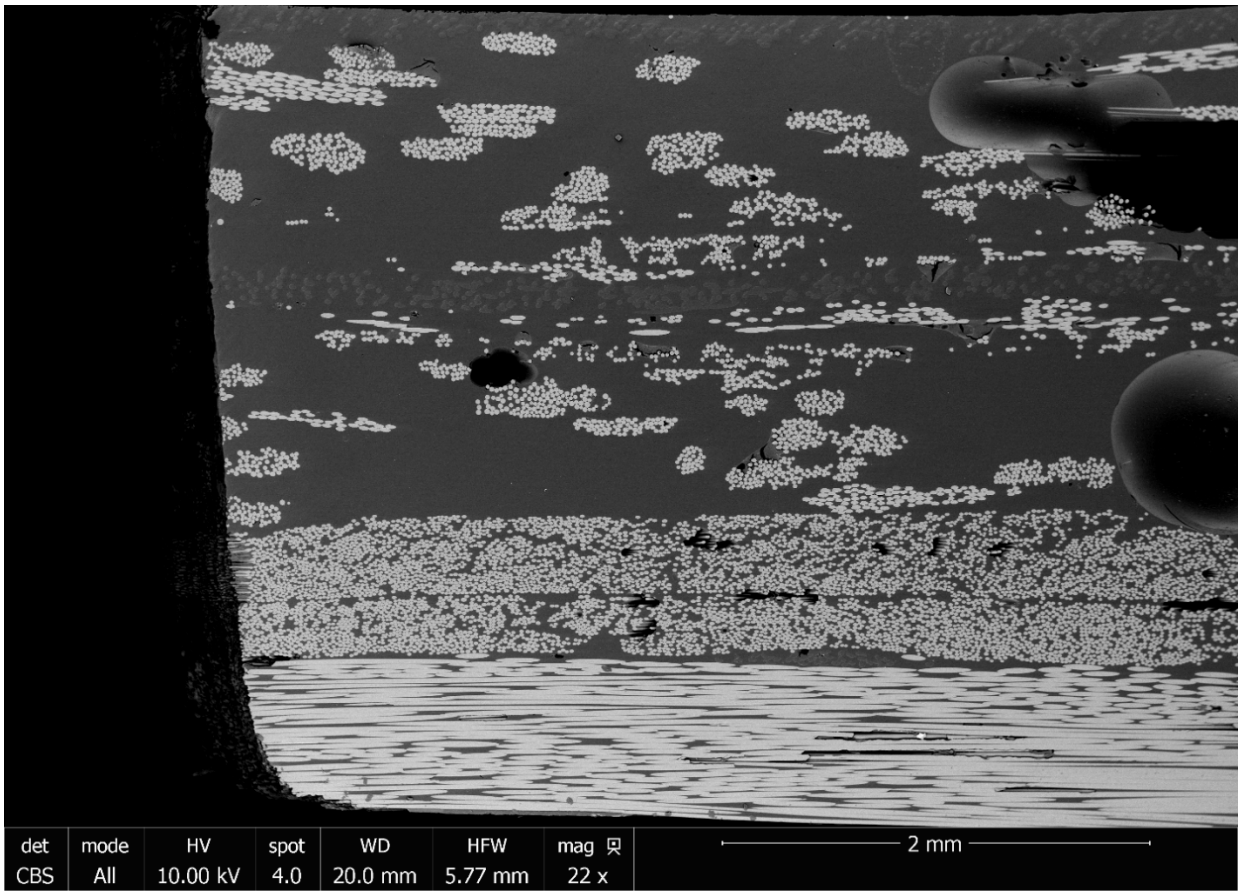

Figure 42. Scanning Electron Microscope Imaging of Mildly Polished Sample

This leads to the disadvantage of SEM and optical imaging, where only the surface of the sample can be studied. If the surface contains irregularities compared to the rest of the material, this will lead to incorrect conclusions. One laborious way to handle this is by slicing the specimen into thin layers and applying these techniques with each of them. However, XCT, a nondestructive method, was used to scan the volume of the specimens.

XCT

XCT is a nondestructive technique used to create 3D geometry of the hidden features of solid objects. This involves focusing X-rays at an object from multiple angles and measuring the variation in the radiation intensity at the detectors. The resulting data are used to reconstruct the distribution of X-ray attenuation through the volume of the scanned object. The resolution of the resulting image depends on the X-ray energy, acquisition time, and size of the object and detectors, but it is much smaller compared to SEM imaging resolutions.

Figure 43 shows images of the longitudinal sections with distinct visualization of the fiber mat orientations. The resolution was more than adequate, displaying particles as small as fiber strands. The outer layer of the FRP sample was scanned to check for actual fiber content, as shown in Figure 44. There were random fiber clumps present in the outer resin layer, but there were no fiber mats. These could have been residues from the fiber mats. Thus, their influence on the tensile strength is miniscule.

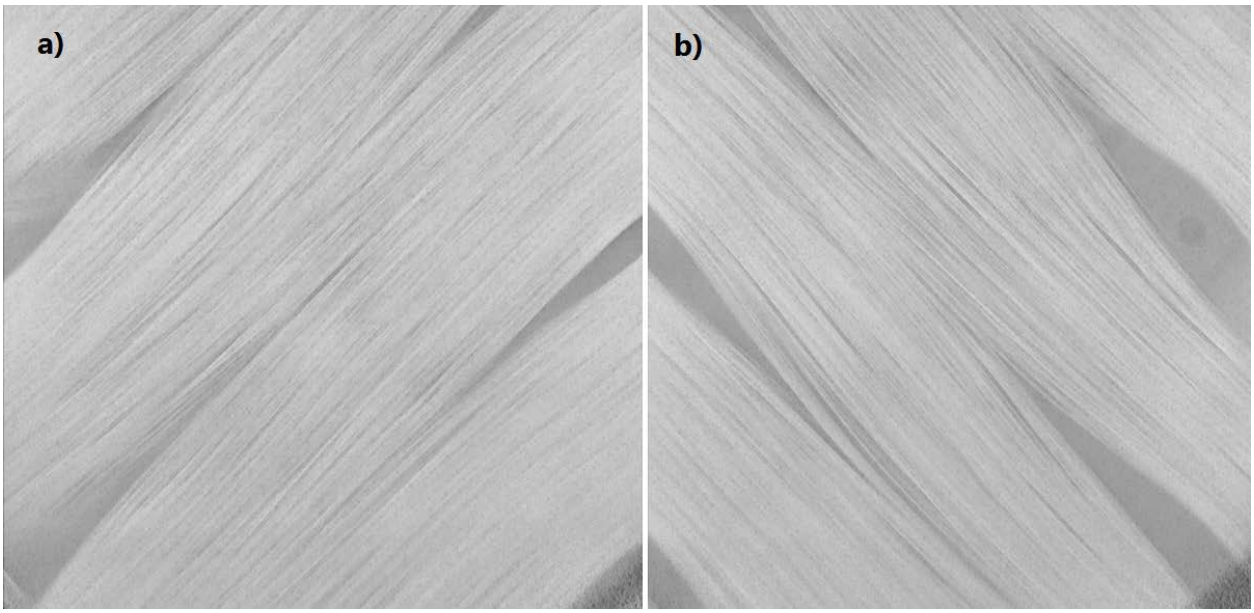

Figure 43. X-ray Computed Tomography Imaging of Fiber Mats: (a) at 45 degree angle; (b) at 135 degree angle

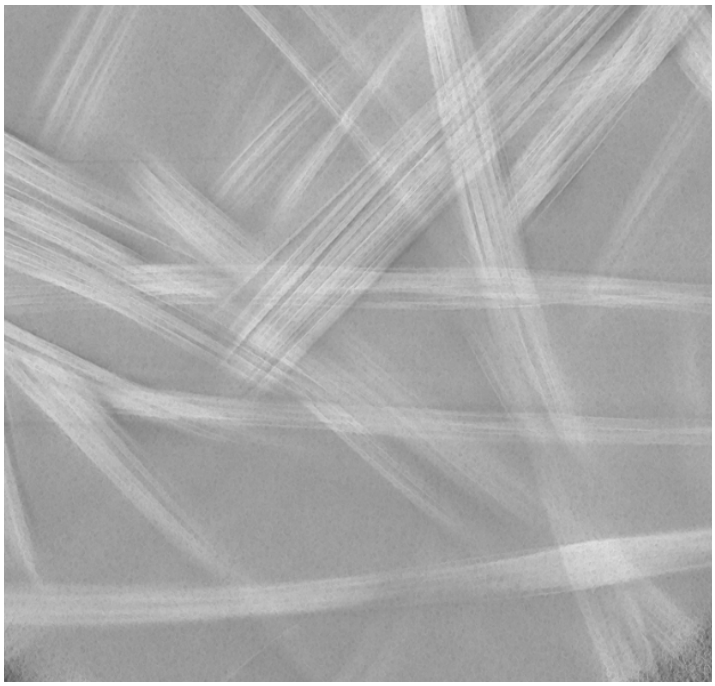

Figure 44. X-ray Computed Tomography Imaging of Random Fiber Clumps at Outside Layer of Fiber-Reinforced Polymer

Tensile Testing

The tensile loads in the HCB are still being carried by the strands in the bottom, whereas the fibers carry the shear load from traffic by means of 45° rotated orientation. However, tensile testing was selected for characterizing the FRP specimens because of the ease and simplicity of testing. Thus, the tensile test results for the FRP specimens should not be taken directly as a

substitute for shear strength, rather only as an indication of its contribution. Three specimens were selected from each exposure site and laboratory. Dog-bone shaped specimens were fashioned to meet the requirements of ASTM D638, Type IV (ASTM, 2014). These specimens (shown in Figure 45) were tested for ultimate tensile strength.

The results and specimen dimensions are shown in Table 3. L# and LO# specimens are unexposed and exposed (2000 hr of accelerated exposure) laboratory specimens, respectively. HB# and HR# specimens are field exposure specimens from Harrisonburg and Hampton Roads, respectively. A strong relationship between the specimen thickness and ultimate tensile strength was found, with $R^2 = 0.85$, as shown in Figure 46. No other correlation existed. This indicates that the tensile strength depends mainly on the thickness or the fiber content in the cross section. From the thickness and tensile strength, the specimens can be separated into two categories: LO# or thick specimens (shown as bold in Table 3), and the rest of the thin specimens.

Figure 45. ASTM D638 Type IV Dog-bone Fiber-Reinforced Polymer Specimens

Table 3. Tensile Testing Results

Sample ID	Force (lb)	Cross-section Area (in^2)	Width (in)	Thickness (in)	Ultimate Tensile Strength (ksi)
LO1	2060	0.056	0.25	**0.224**	**36.9**
LO2	1796	0.051	0.25	**0.204**	**35.1**
LO3	1401	0.051	0.25	**0.203**	**27.6**
HB3	209	0.033	0.25	0.133	6.3
HB4	224	0.035	0.25	0.139	6.4
HB5	206	0.034	0.25	0.136	6.1
HR1	230	0.035	0.25	0.138	6.7
HR2	217	0.036	0.25	0.142	6.1
HR3	318	0.035	0.25	0.139	9.2
L1	200	0.028	0.25	0.112	7.1
L2	148.7	0.028	0.25	0.110	5.4
L3	230	0.025	0.25	0.099	9.3

Bold type indicates thicker specimens.

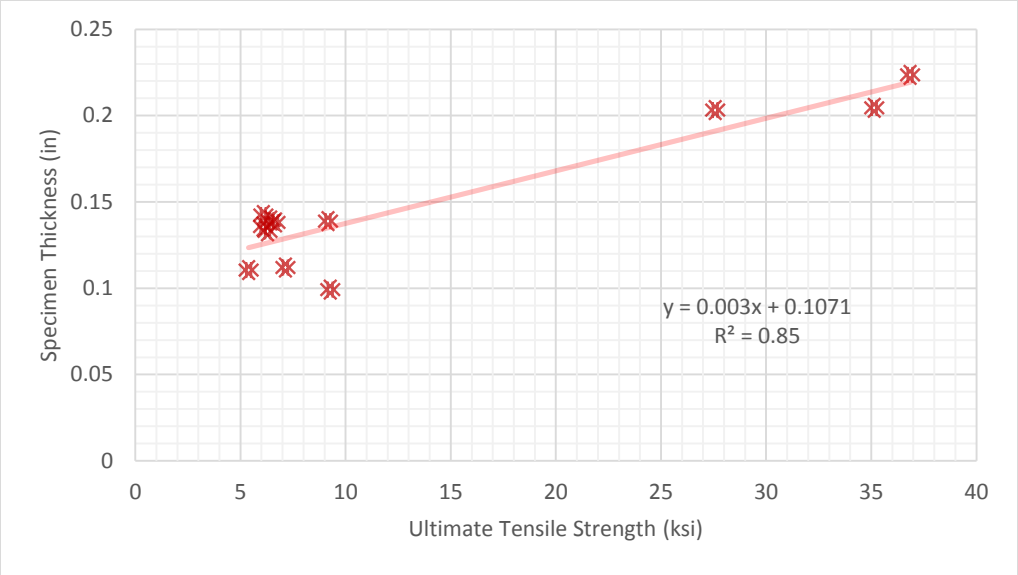

Figure 46. Relationship Between Specimen Thickness and Ultimate Tensile Strength

On average, the thickness of the LO# specimen was 65% greater than that of the rest of the specimens; however, their average tensile strength was about 374% greater. By evaluating the SEM images of the cross sections, it was found that most of the tensile fiber content started at about 0.09 in (2.25 mm) from the outside surface of the FRP specimens. This indicates for the sake of the inspection that if scraping damage is limited to the outer 2 mm or so, the strength of the material will not decrease significantly. However, this finding might apply only to this case, since FRP construction may not be precise enough to have the exact cross section in every beam.

In addition, it was established earlier that the FRP shell acts as an important load-bearing member; thus, the fiber content in the shell, being the principal tensile load-carrying material, must be preserved for structural integrity and expected load-carrying performance. Thus, any fiber exposure must be sealed because of resin degradation as soon as possible for durability.

Corrosion Possibility in Strands

Corrosion of the tension-tie strands is a concern, since the unstressed strands in the beam bottom are only minimally embedded in concrete at their ends, which protects the steel with high pH levels. Fortunately, in HCBs, the strands are embedded in a thin layer of vinyl ester resin in all directions, as seen in Figure 1b. In case of moisture leakage from the top into the FRP shell, either from the concrete deck at the top or from accidental pierced holes in the side web, the moisture would flow through the foam and stagnate on top of the resin layer, which is embedding the strands. Vinyl ester is a highly water-resistant material because of its resistance to hydrolysis reaction, which is why this FRP resin is typically preferred for boat making. Therefore, the resin layer will typically not allow moisture to reach the strands within the structure's design life.

In the event of an extreme case of piercing damage from the bottom that compromises the resin layers surrounding the strands during a flood event, moisture and oxygen may become available to the strands. This can initiate corrosion, but the extent of exposure will determine the

rate of corrosion reaction. In addition, corrosion will proceed only while moisture is available. If the steel strands eventually dry out, the corrosion reaction will slow down or come to a stop. Therefore, unless the strands are exposed to moisture, corrosion should not affect the integrity of the strands in the HCB.

CONCLUSIONS

- *None of the composite beam components exhibited complete failure after 1 year and 8 months of outdoor atmospheric exposure. Therefore, for understanding the full degradation behavior, a longer duration of environmental exposure is needed.*

- *GPR can detect even trivial amounts of moisture content with good sensitivity in the interior of an HCB.*

- *If performed periodically, spectrocolorimeter readings can provide extensive information on the aging behavior of FRP shell specimens.*

- *FTIR can provide in-depth, molecular bond–level information on the chemical structure of FRP. However, FTIR can be used only as a research tool for special cases, because of the complexity in the interpretation of the results, not as a routine inspection technique.*

- *Accelerated laboratory UV exposure served as a valuable way of simulating degradation of FRP specimens, especially for the beginning stages of deterioration. However, when followed through, the accelerated exposure could lead to unnaturally aggressive exposure conditions compared to true environmental exposure, which then leads to an unnatural degradation behavior in the later stages of deterioration.*

- *Loss of surface resin and subsequent exposure of tensile fiber are more likely to occur in the FRP material because of freeze-thaw cycles and scraping damages during flood events and freeze-thaw cycles. Loss of tensile fiber mats can reduce the carrying capacity of the FRP.*

- *Corrosion of strands in the beam bottom is less likely because of the embedding resin unless moisture penetrates the resin layers.*

RECOMMENDATIONS

1. *VDOT's Structure and Bridge Division should prescribe periodic protective UV coatings on the FRP surface of the exterior of HCBs.*

2. *VDOT's Structure and Bridge Division should implement GPR as an inspection tool to detect moisture inside HCBs in use in VDOT structures. The presence of moisture indicates a breach of the FRP shell, and the breach needs to be repaired to prevent further moisture penetration.*

3. *The Virginia Transportation Research Council (VTRC) should continue to monitor the HCB specimens at the Hampton Roads and Harrisonburg exposure sites for rate of degradation.*

4. *VDOT's Structure and Bridge Division should prescribe inspection of the HCBs for resin losses because of exposure and/or scraping damages on the FRP material in HCBs and immediately repair the lost section using epoxy-like material to avoid damage to the load-carrying glass fibers.*

5. *VTRC should evaluate the HCB bridge in VDOT's Fredericksburg District with GPR for the presence of moisture and drill a drain hole at a low point in the bottom to verify the presence of moisture and provide for drainage.*

6. *VDOT's Structure and Bridge Division should pause further use of HCBs since there are still many unknowns about the late-stage deterioration mechanism of FRP and since neither visual nor nondestructive methods can fully assess the condition of the beams at this time.*

IMPLEMENTATION AND BENEFITS

Implementation

- Regarding Recommendation 1, for the FRP surface exposed to the sun, VDOT's Structure and Bridge Division will prescribe an established UV-resistant coating material to be applied according to the manufacturer's instructions.

- Regarding Recommendation 2, by June 2020, the VDOT Structure and Bridge Division's Inspection Team will specify GPR for detecting moisture penetration inside the FRP shell after flood events.

- Regarding Recommendation 3, VTRC will periodically monitor the field exposure specimens to keep track of the deterioration behavior of the specimens until severe deterioration occurs.

- Regarding Recommendation 4, by June 2020, VDOT's Structure and Bridge Division will specify resin repair techniques in the event of resin degradation.

- Regarding Recommendation 5, VTRC will work with VDOT's Fredericksburg District to conduct a field evaluation of the HCB bridge by December 2019.

- Regarding Recommendation 6, no further action needs to be taken.

Benefits

- Regarding Recommendation 1, UV radiation was concluded to be the most damaging factor for the FRP shell in the HCB. Thus, periodically coating the beams with protective UV

coatings will slow down the UV-induced degradation. This will provide a longer service life for HCB bridges.

- Regarding Recommendation 2, GPR proved to be a reliable tool to detect even minor amounts of moisture inside HCBs. By implementing this nondestructive evaluation technique, any leakage source can be detected and repaired in the early stages. This is a crucial inspection need for this type of bridge superstructure, without which no other method exists to warn VDOT of impending deterioration. By detecting moisture earlier in the deterioration cycle and treating the problem, safety of traveling public can be assured and expensive late-stage rehabilitation or replacements, which can cost hundreds of thousands of dollars, can be avoided.

- Regarding Recommendation 3, 1 year and 8 months proved to be a short duration for the degradation of the HCB specimens. The specimens should be monitored periodically for signs of degradation. This will provide a reliable set of data to predict the service life of HCB bridges.

- Regarding Recommendation 4, this preventive measure can ensure the durability of HCBs by addressing problems with resin degradation well before the load-carrying fibers are exposed and damaged. This preventive technique will save VDOT maintenance money and effort in the long run.

- Regarding Recommendation 5, this will validate the GPR's ability to detect moisture inside HCBs in a field environment and will verify if there is corrosion in the strands.

- Regarding Recommendation 6, since there are many unknowns left about the deterioration mechanism of FRP, it will be safer to pause construction of HCB bridges until further information on the deterioration mechanism is available.

ACKNOWLEDGMENTS

The authors thank Dennis Huffman at Virginia Tech for providing specimens from HCBs; Tray Lee for helping with the exposure rack designs; Bill Ordel for fashioning the specimens and monitoring the field exposure specimens; Joseph Thompson for assisting with the FTIR scans and SEM imaging; and Marlene Wartenberg for assisting with XCT imaging.

REFERENCES

Aboelseoud, M.A., and Myers, J.J. Finite-Element Modeling of Hybrid Composite Beam Bridges in Missouri. *Journal of Bridge Engineering*, Vol. 20, No. 1, 2015.

Ahsan, S. *Evaluation of Hybrid-Composite Beam for Use in Tide Mill Bridge*. Thesis. Virginia Polytechnic Institute and State University, Blacksburg, 2012.

ASTM International. *ASTM D4587-11: Standard Practice for Fluorescent UV-Condensation Exposures of Paint and Related Coatings.* West Conshohocken, PA, 2011.

ASTM International. *ASTM D638-14: Standard Test Method for Tensile Properties of Plastics.* West Conshohocken, PA, 2014.

Davis Instruments. *Vantage Pro2 Console User Manual.* Hayward, CA, 2014.

Hillman, J.R. *Investigation of a Hybrid-Composite Beam System*. Transportation Research Board, Washington, DC, 2003.

Hillman, J.R. *Product Application of a Hybrid-Composite Beam System*. Transportation Research Board, Washington, DC, 2008.

Harris, D.K., and Civitillo, J.M. *In-Service Performance Evaluation and Monitoring of a Hybrid Composite Beam Bridge System.* VTRC 18-R5. Virginia Transportation Research Council, Charlottesville, 2017.

Schwiegerling, J. *Field Guide to Visual and Ophthalmic Optics.* SPIE Press, Bellingham, WA, 2004.

Signor, A.W., VanLandingham, M.R., and Chin, J.W. Effects of Ultraviolet Radiation Exposure on Vinyl Ester Resins: Characterization of Chemical, Physical and Mechanical Damage. *Polymer Degradation and Stability*, Vol. 79, No. 2, 2003, pp. 359-368.

Telang, N.M., Dumlao, C., Mehrabi, A.B., Ciolko, A.T., and Gutirrez, J. *Field Inspection of In-Service FRP Bridge Decks*. Transportation Research Board, Washington, DC, 2006.

U.S. Department of Transportation. *2015 Status of the Nation's Highways, Bridges, and Transit: Conditions & Performance*. Washington, DC, 2015.

Van Nosdall, S., Moen, C., Cousins, T., and Roberts-Wollmann, C. Experiments on a Hybrid-Composite Beam for Bridge Applications. *Transportation Research Record: Journal of the Transportation Research Board,* No. 2332, 2013, pp. 43-52.

Virginia Department of Transportation. *Guide Manual for Causes and Repair of Cracks in Bridge Decks*. Richmond, 2009.

Visco, A.M., Brancato, V., and Campo, N. Degradation Effects in Polyester and Vinyl Ester Resins Induced by Accelerated Aging in Seawater. *Journal of Composite Materials*, Vol. 46, No. 17, 2012, pp. 2025-2040.